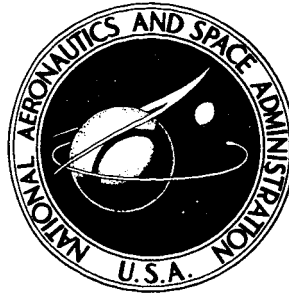


~~RESTRICTED DATA~~
ATOMIC ENERGY ACT OF 1954

**NASA TECHNICAL
MEMORANDUM**



UB
NASA TM X-1471

UB
NASA TM X-1471

CLASSIFICATION CHANGED

To Unclassified

By authority of H. H. Marier

Date Jan. 3, 1973
per lmd

**STARTUP HEAT-TRANSFER AND
FLUID-FLOW CHARACTERISTICS IN
A NUCLEAR-ROCKET REFLECTOR**

*by Francis C. Chenoweth, Eugene J. Pleban,
John S. Clark, and Earl L. Sprague*

*Lewis Research Center
Cleveland, Ohio*

NOV 09 2004

STARTUP HEAT-TRANSFER AND FLUID-FLOW CHARACTERISTICS
IN A NUCLEAR-ROCKET REFLECTOR

By Francis C. Chenoweth, Eugene J. Pleban,
John S. Clark, and Earl L. Sprague

Lewis Research Center
Cleveland, Ohio

RESTRICTED DATA

ATOMIC ENERGY ACT OF 1954

GROUP 1

Excluded from automatic
downgrading and declassification

CLASSIFIED DOCUMENT—TITLE UNCLASSIFIED

This material contains information affecting the national defense of the United States within the meaning of the espionage laws, Title 18, U.S.C., Secs. 793 and 794, the transmission or revelation of which in any manner to an unauthorized person is prohibited by law.

NOTICE

This document should not be returned after it has satisfied your requirements. It may be disposed of in accordance with your local security regulations or the appropriate provisions of the Industrial Security Manual for Safe-Guarding Classified Information.

NATIONAL AERONAUTICS AND SPACE ADMINISTRATION

~~CONFIDENTIAL~~

STARTUP HEAT-TRANSFER AND FLUID-FLOW CHARACTERISTICS IN A NUCLEAR-ROCKET REFLECTOR (U)

by Francis C. Chenoweth, Eugene J. Pleban,
John S. Clark, and Earl L. Sprague

SUMMARY

The accurate prediction of transient heat-transfer and fluid-flow characteristics is vital to the development of a nuclear-rocket reflector system. Presented herein are (1) an analytical procedure that may be used to calculate fluid conditions and material temperatures as a function of time and position, (2) a description of a nuclear-rocket cold-flow simulator experiment performed at the Lewis Research Center, and (3) a comparison of experimental and predicted reflector data obtained by using experimental reflector-inlet and initial-material temperature data as input to the prediction program.

Predicted reflector-exit pressures were within about 12 percent of the experimental data. Reflector pressure-drop results showed rather abrupt discontinuities consistent with the input data but were, for the most part, within about 20 percent of experimental data. Exit plenum fluid temperature predictions were generally within about 6 percent or 31° R; however, the predicted temperature at some individual passage exit did not compare as well.

A comparison of predicted and experimental material temperatures indicated predicted temperatures higher than experimental near the graphite inner reflector cylinder and lower than experimental near the pressure vessel. This shift in the temperature level was apparently caused by assuming that the inlet pressure and enthalpy were the same for each passage in the prediction program. The actual pressure and enthalpy at the reflector inlet were a function of the radial position; however, there was not enough experimental data in this area to determine the relations.

Poor agreement between predicted and experimental material temperature was observed because the predicted heat-transfer coefficients in the transition region from two-phase to single-phase flow exhibited a discontinuity that resulted in unusual axial temperature profiles. More experimental work is required to obtain a continuous correlation in this area.

INTRODUCTION

The development of nuclear-rocket systems requires the definition of performance

~~CONFIDENTIAL~~

[REDACTED]

characteristics for all modes of operation in the various components of the system. One of the most complex of these components is the reflector assembly in which a relatively large mass of material is convectively cooled by hydrogen flowing through a number of circular and irregularly shaped coolant passages.

Temperature gradients due to transient conduction can cause significant thermal stresses and strains in a reflector assembly that may interfere with the mechanical operation during a reactor startup. A method of predicting reflector material temperatures during these transients is necessary to perform stress analyses and assure permissible strain levels within the reflector. Also, it is important that the density of the reflector effluent be well known during the startup transient, as well as during full-power and shutdown conditions, since excess hydrogen density at the reactor-core inlet may cause an undesired increase in core reactivity. Furthermore, reflector pressure drop is a significant part of the total system pressure drop during the startup transient and must be known in order to determine pumping requirements. Finally, it is apparent that a method of predicting transient heat-transfer and fluid-flow characteristics would be useful to evaluate different designs or to compare various operating modes (different flow rate ramps, power ramps, etc.)

An iterative numerical procedure capable of predicting these performance characteristics is presented in this report. Several uncertainties are involved in the development of an analytical procedure of this type, however, including (1) the selection of the appropriate heat-transfer and pressure-drop correlation (gaseous and two phase), (2) mathematical model used to represent the geometrical shape of the reflector, (3) boundary conditions, and (4) flow asymmetries.

In reference 1, the first of these uncertainties was isolated by considering a single-tube experiment and evaluating several existing correlations. The inside diameter, heat-transfer surface area, and mass of the single tube used in the experiments were selected to simulate a typical circular passage in a nuclear-rocket reflector. This report discusses the other uncertainties in items (2) to (4). In an attempt to determine the significance of these uncertainties, the results of the numerical procedure are compared with experimental data obtained at Lewis.

Two similar procedures have been reported. Aerojet-General Corporation, the NERVA (Nuclear Engine for Rocket Vehicle Application) prime contractor, has presented a complete system analysis (ref. 2) that includes the reflector system. Geometrically similar coolant passages are grouped together; heat-transfer and fluid-flow characteristics are assumed to be the same in all passages in a group. The program has a capacity for five different groups and up to ten axial increments in any component. The analysis includes two-phase and gaseous heat transfer and calculates fluid and coolant-wall temperature distributions; internal material temperatures (which are required for any stress analysis) are not calculated.

~~CONFIDENTIAL~~

Westinghouse Astronuclear Laboratory (the NERVA engine subcontractor) has developed and reported (ref. 3) a procedure similar to the analysis presented in this report (a multichannel, heat-transfer, and fluid-flow code, coupled with a modified TØSS program (ref. 4)). The Westinghouse analysis is limited to the all-gas region, however.

The analysis presented in this report considers both two-phase and gaseous-hydrogen flow. Also, internal material temperatures are calculated at 31 internal nodes and 13 axial increments (403 internal nodes). A 15° repeating section of the reflector is considered in the calculations. Also, 33 flow passages and 55 wall temperatures are considered for each axial increment. Thus, the merit of the prediction code described in this report lies in the fact that it yields a detailed map of flow rates, temperature distribution, and pressures throughout the reflector system.

A full-scale cold-flow nuclear-rocket simulator experiment was conducted at the Plum Brook Station of the Lewis Research Center. One of the many specific objectives of the experimental program was to obtain data to verify and/or improve calculation methods for predicting component pressure drops, fluid properties, and material temperatures as a function of time.

A description of the facility and turbopump and a comparison of predicted and experimental turbopump data are presented in reference 5. Reference 6 presents predicted and experimental data obtained from the simulated reactor core. Reference 7 presents similar results for the nozzle used on the facility, and reference 8 discusses the problem of calculating flow rates and fluid states at the various interfaces within the system.

Presented herein are (1) a description of the reflector system used in the nuclear rocket simulator experiments at Plum Brook, (2) experimental data obtained from the experiments, (3) comparisons of predicted and experimental results (obtained by using the reflector-inlet conditions and initial-material temperature as input data to the prediction program), and (4) a discussion of the results and limitations of the program.

APPARATUS

A schematic diagram of the research apparatus is presented in figure 1. The system is filled to the pump main discharge valve and cooled to liquid-hydrogen temperature prior to the test. Liquid-hydrogen flow is started by the controlled opening of the pump main discharge valve. Hydrogen flows from the 2000-gallon run tank, through the turbine-type flowmeter and into the turbopump. From the turbopump, the liquid hydrogen is forced through the venturi meter, the pump main discharge valve, and into the 4-inch propellant feed line. The hydrogen picks up sensible heat from the components of the system downstream of the pump main discharge valve. From the 4-inch feed line,

[REDACTED]

the flow enters the nozzle-inlet spider, and then the regneratively cooled nozzle. From the nozzle-coolant tubes, the hydrogen enters the reflector-inlet plenum, mixes, and again separates as it passes through the reflector-coolant passages. On leaving the reflector passages, the hydrogen reverses direction around the reactor dome, passes through a flow separator and core support plate and enters the core coolant passages. Finally, the hydrogen flows from the core coolant passages into the nozzle chamber, through the nozzle throat, and is exhausted into the facility vacuum exhaust duct. A detailed description of the facility and test procedure is presented in reference 5. References 6 and 7 also present summaries of the test procedure.

Reflector Assembly

A schematic diagram of the reactor used in the nuclear rocket simulator experiments is presented in figure 2. The nuclear reactors currently being developed in the NERVA program contain graphite fuel elements (fueled beads are embedded in the graphite) and a beryllium reflector. Since the graphite elements used in the core of the simulator experiment at Plum Brook were not fueled, nuclear shielding was not required. Also, the high cost of a beryllium reflector motivated a search for a substitute material. Calculations indicated that an aluminum reflector provided similar cooldown characteristics during the startup portion of the run. Thus, the reflector used in these experiments was made of aluminum. Similarly, the control drums and poison plates are aluminum simulations.

The physical relation of the various reflector components can be noted in figure 2. The components are listed as follows:

- (1) Reflector cylinder: graphite
- (2) Impedance ring: flow restriction in the annulus between the graphite inner-reflector cylinder and the outer reflector
- (3) Reflector segment: or outer reflector, manufactured in four axial pieces
- (4) Control drums: manufactured in four axial pieces
- (5) Tie rods: hold control drums in position
- (6) Pressure vessel: contains the entire reactor assembly

Since nuclear control of the reactor was unnecessary, no provision was made for external movement of the control drums.

Figure 3(a) shows four of the aluminum outer-reflector segments, and figure 3(b) shows the simulated control drum and poison plate, before assembly. Figure 4 shows one assembled sector (12 sectors make up the complete outer reflector) of the aluminum outer reflector. Some of the instrumentation leads are shown in figure 4 as they were attached. Figure 5 shows the outer-reflector assembly after the 12 sectors were

[REDACTED]

assembled on the assembly stand. Figure 6 shows the lowering of the dome and pressure vessel assembly over the outer-reflector assembly. Finally, the pressure vessel and outer-reflector assembly were lowered over the graphite core and inner-reflector assembly, as shown in figure 7. Reference 6 gives details of the graphite core assembly.

Instrumentation

The positions of the instrumentation for the runs considered in this report are illustrated in figures 8 to 11. Figure 8 shows the instrumentation at the reflector-inlet plenum; section A-A illustrates the complexity of the flow patterns at the reflector inlet. Figure 9 shows the location of the static pressure taps within the reflector. Similarly, figure 10 presents the location of the thermocouples that were installed to measure the reflector material temperatures. Three fluid temperature measurements within the control-drum slot were recorded on one of the runs, and the location of these sensors is also shown in figure 10. Finally, figure 11 shows the instrumentation at the reflector-outlet plenum.

The following symbols are used to identify the instrumentation:

- RP - reactor pressure
- RT - reactor temperature (thermocouple)
- RR - reactor temperature (resistance probe)
- RM - reactor temperature (platinum film probe)

These designations are consistent with the designations used in references 6 to 8.

The data acquisition system is described in reference 6. The data discussed in this report were recorded on the 4 or 10 kilocycle digital recording equipment and were converted from millivolt data to engineering units (temperatures, pressures, etc.) on the Lewis modified Univac computer.

Estimates of the accuracy of the various instrumentation measurements are presented in references 6 to 8. A summary of the estimate of the accuracies of the measurements made in the reflector system are shown in table I.

In this report, transient response errors have been neglected (ref. 8 discusses this problem in detail). The platinum-film resistance temperature probes, which were used to measure fluid temperatures within the control-drum slots, were selected to yield very fast response temperature data. A very thin film of platinum was deposited on a ceramic plug, and the instrumentation leads were attached to each side of the film. The ceramic plug was then cemented to a larger bakelite plug which was, in turn, attached to the simulated poison plate. A hole was milled in the simulated poison plate so that the platinum film was approximately flush with the outer surface of the poison plate. Because the mass of the platinum film is small, the temperature of the film varies

[REDACTED]

TABLE I. - ESTIMATES OF MEASURE-
MENT ACCURACY

| Type | Range | Estimated accuracy |
|--------------------------------|--|--|
| Copper-constantan thermocouple | 660 ⁰ to 385 ⁰ R 385 ⁰ to 100 ⁰ R Below 160 ⁰ R | ±0.75 ⁰ R ±1 Percent No estimate |
| Pressure transducers | All | ±1 Percent of full scale |
| Flowmeter | 0 to 14 lb/sec Above 14 lb/sec | ±2 Percent No estimate |
| Calculated nozzle flow rate | All | No estimate |
| Resistance temperature probe | 20 ⁰ to 540 ⁰ R 20 ⁰ to 60 ⁰ R | ±9 ⁰ at 40 ⁰ R ±0.4 ⁰ at 40 ⁰ R |
| Platinum-film probe | 30 ⁰ to 600 ⁰ R | No estimate |

approximately as the temperature of the fluid flowing past the film. It is important to recognize that these platinum-film resistors were, in a sense, experimental instrumentation. No estimate of the accuracy of this type of transducer has been made; the results obtained from them, however, are discussed further in the section RESULTS AND DISCUSSION.

ANALYTICAL PROCEDURE

Concurrent with the physical operation of the facility described in the preceding section and in references 5 to 8, an effort was made to predict analytically fluid and material temperatures and fluid-flow parameters in the various components of the reflector system. This section concerns itself with the calculation details of a multi-passage flow and heat-transfer prediction code. (Symbols are defined in appendix A.)

The prediction program is in two main parts, (1) Reflector Analysis Fluid Flow (RAFF) and (2) Transient or Steady-State Temperature Distribution (TØSS). A FORTRAN IV version of TØSS was modified to accept RAFF in its overlay structure and to consider material thermal conductivity k and specific heat C_p variables with respect to temperature. RAFF is an extension of the code described in reference 1, which has only single-tube capabilities. A hydrogen fluid-properties subroutine STATE(J) (ref. 9) is included in RAFF. The code is written for general use and, therefore, can be used for other geometries and systems that use hydrogen as the operating fluid. (A fluid change can be made by modifying RAFF and substituting a

CONFIDENTIAL

fluid-properties subroutine for STATE(J).)

Heat-transfer geometry and initial material temperatures are input to TØSS. Flow-passage geometry and initial experimental mean fluid temperatures and pressures at the reflector inlet over a time interval are input to RAFF. RAFF explicitly and iteratively solves basic conservation-of-flow equations and convection heat-transfer equations for mean fluid temperatures and pressures and for mean heat-transfer coefficients at all passage stations. With the quasi-steady-state map of fluid-boundary conditions from RAFF, TØSS solves a set of heat-diffusion differential equations for material and surface temperatures of the reflector system at successive time increments to the end of the time interval. Computer flow diagrams are presented in figures 12 and 13.

Reflector Analysis Fluid Flow (RAFF)

The multipassage fluid-flow code RAFF is based on the calculational procedure given in appendix B that describes the formulas used to determine hydrogen fluid pressures and temperatures in the coolant passages along the length of the reflector. Initial conditions are a quasi-steady-state map of average wall temperatures along the length of each passage and a set of initial inlet-plenum fluid conditions obtained from either actual measurements or predicted values. The hydrogen-properties routine STATE(J) is used to calculate transport properties as needed by RAFF.

Assumptions. - The basic assumptions used in deriving the continuity equations for the flow network are as follows:

(1) The bulk temperature used to determine the heat flux Q for each increment of a passage is the average of the inlet and exit temperatures for the increment.

(2) The flow of hydrogen is adjusted to prevent calculated negative pressures in the passages.

(3) Any fluid entering the exit plenum has experienced the same pressure drop across all the passages.

(4) The flow in a passage is considered one dimensional.

(5) The flow rate is constant over the length of a passage.

(6) The wall temperature used to determine the heat flux Q at the boundaries is the average of all the surface-node temperatures adjacent to the passage increment.

Heat-transfer coefficients. - Passage calculations for the heat flux Q were based on fundamental laws of convective heat transfer and turbulent fluid flow. A general discussion of heat-transfer coefficients and their use in single-tube, fluid-flow computations is given in reference 1. As a result of reference 1, the following correlations were selected to be used in this code.

For a fluid in the gas region (quality ≥ 0.90), a modified Seider-Tate heat-transfer

CONFIDENTIAL

correlation was used in the following form:

$$h_g = 0.021 \frac{k}{D} Re_b^{0.8} Pr_b^{0.4} \left(\frac{T_w}{T_b} \right)^{-0.575} \quad (1)$$

The fluid properties k , Re , and Pr were based on the average pressure and bulk temperature of the fluid associated with a passage increment (ref. 10). The exponent on the Prandtl number was changed from $1/3$ to 0.4 consistent with current practice when the heat transfer is from the wall to the gas (ref. 11). The modified Seider-Tate correlation was selected for this study since it was shown in reference 1 to yield satisfactory results.

For a fluid in the two-phase region ($0.05 < \text{quality} < 0.90$) the Hendricks, et al. (ref. 12) correlation was used in the following form:

$$h_{2\phi} = \frac{0.023 \frac{k}{D} Re_f^{0.8} Pr_f^{0.4}}{0.611 + 1.93 \chi_{tt}} \quad (2)$$

The fluid properties were based on average pressure and film temperatures associated with a slug of two-phase fluid in an increment. The use and calculation of the Martinelli parameter χ_{tt} and the correlation in equation (2) is given in reference 12 and in appendix B. Starting values were based on instantaneous inlet values of pressure and bulk temperature after entrance losses.

Pressure-drop equations. - Pressure-drop calculations were based on equations given in appendix B. Entrance and exit losses were included. It is possible, by using these procedures, to calculate negative pressure in any or all the parallel passages. Calculated negative pressures were handled in two ways. (1) If all the passages yielded calculated negative pressures, the flow rate was reduced by 2 percent and the calculations restarted. (2) Otherwise, the flow rate in each passage was redistributed according to equation (B17).

This procedure allows the calculations to proceed on the computer. Flow rate values are obtained from experimental results and are very uncertain, especially during the first time increment; storage of hydrogen may occur between the reflector inlet and the nozzle chamber.

Convergence. - The basis of convergence within a passage increment was the relative error between successive values of the heat flux from the passage wall to a slug of coolant fluid. An arbitrary value of 2 percent relative error was used. The basis of convergence within a particular time increment, which signals the transfer to TØSS, was the relative error between the maximum and minimum values of the exit pressures

from all the passages. An arbitrary value of 3 percent relative error was used.

On convergence, values of turbulent-flow convective heat-transfer coefficients (h_g , $h_{2\phi}$) are made available to TØSS. Calculated coolant fluid temperatures along the length of each passage are also made available to TØSS for the next transient time increment.

Geometry considerations. - Two coolant-passage geometries are considered: slotted and circular. Slotted passages may contain a restriction at any station along the length. The pressure drop across the restriction is defined by a head loss coefficient (which, in this case, was determined experimentally) and the restricted area. For each circular passage a different diameter may be specified. A width and length is required for each slotted passage. The hydraulic diameters are used to calculate heat-transfer characteristics for the slots.

The length of the increments of a passage used in this study was 4 inches, a limit based on the availability of computer storage. Longer lengths may be prescribed; however, no attempt was made to evaluate the effect of variable increment lengths on the overall solution.

Transient or Steady State (TØSS)

The temperature calculation code TØSS is based on a calculational procedure developed in reference 4. The calculations consist of stepping through time in increments of $\Delta\tau$ and solving the explicit form of the first forward finite-difference expression for a general form of the heat-diffusion equation applied in three dimensions (x, y, and z) for each node.

$$\frac{\partial}{\partial x} \left[k(T) \frac{\partial u}{\partial x} \right] + \frac{\partial}{\partial y} \left[k(T) \frac{\partial u}{\partial y} \right] + \frac{\partial}{\partial z} \left[k(T) \frac{\partial u}{\partial z} \right] = \rho C_p(T) \frac{\partial u}{\partial \tau} \quad (3)$$

where

$$u = T(\tau)$$

Assumptions. - The basic assumptions used in deriving the explicit finite-difference form of the thermal equation are as follows (ref. 4):

- (1) In calculating the change of temperature of any node for a small time interval, only that node and its adjacent nodes are considered.
- (2) The temperature at any node is the average temperature over its own increment.
- (3) The initial rate of temperature change for any time interval is constant over the whole interval.

[REDACTED]

Heat-transfer calculations. - The explicit finite-difference form of equation (3) without internal heat generation (ref. 4) is

$$\frac{\Delta\tau}{C_q} \sum_p T_p(\tau) Y_{pq} = \Delta T_q \quad (4)$$

where p denotes all neighboring nodes of internal node q and q itself, and Y_{pq} represents the reciprocal of the heat-transfer resistance between either adjacent internal nodes or surface-to-internal nodes. The boundary effect is transmitted to the internal node by virtue of the heat-transfer coefficient between boundary and surface nodes.

Equation (4) is written for each internal node q and is solved directly for ΔT_q , and, subsequently,

$$T_{q,\tau} + \Delta\tau = T_{q,\tau} + \Delta T_q$$

The updated temperature of node q is then used for the next time increment.

This procedure is continued until the end of a specified time interval is reached, at which time new flow parameters (T_w , etc.) are computed and sent on to RAFF. During this time interval, the mean boundary coolant temperatures and heat-transfer coefficients that were updated by RAFF are considered constant.

Stability. - The explicit solution of the set of equations is stable under certain conditions on $\Delta\tau$ for all internal nodes q . The stability relation from reference 4 is

$$\Delta\tau_{\max} = \left(-\frac{C_q}{Y_{pq}} \right)_{\min} \quad (5)$$

Conditions for overall stability were not investigated.

Geometry considerations. - In mathematical description of the inner and outer reflectors for TØSS, each node is considered to be a parallelepiped. A length, width, and depth must be specified that determine the volume V of the node. Since the volume and depth of each node were well known, the lengths and widths were easily calculated to simulate the actual volumes. The conducting areas and lengths between nodes (internal to internal or surface to internal), however, were not easily defined, particularly when the internal node contained a hole. Tables II and III list the node and connector dimensions used in this study. No attempt was made to improve the original dimension estimates.

Nodal breakdown of a 15° sector of the reflector is shown in figure 14. Computer

TABLE II. - INTERNAL

NODE DIMENSIONS^a

| Node | Length | Width |
|------|--------|--------|
| 1 | 1.0600 | 0.5000 |
| 2 | 1.4250 | 1.1030 |
| 3 | 1.1295 | .6720 |
| 4 | 1.2720 | .6720 |
| 5 | 1.2720 | .6720 |
| 6 | 1.0640 | 1.0940 |
| 7 | 1.2120 | 1.0940 |
| 8 | 1.2120 | 1.0940 |
| 9 | 1.1150 | .9690 |
| 10 | 1.1490 | .9690 |
| 11 | 1.0260 | .9690 |
| 12 | .4830 | 1.6762 |
| 13 | .4850 | 1.8354 |
| 14 | .9635 | .8120 |
| 15 | 1.0740 | .8120 |
| 16 | 1.0910 | .8120 |
| 17 | 1.0510 | .9520 |
| 18 | 1.0510 | .9520 |
| 19 | .9280 | .9520 |
| 20 | 1.5240 | .5000 |
| 21 | 1.1590 | .5000 |
| 22 | 1.0900 | .5000 |
| 23 | .6860 | .8727 |
| 24 | .7020 | .6981 |
| 25 | .6630 | 1.1115 |
| 26 | .6480 | 1.3900 |
| 27 | .4810 | 1.4600 |
| 28 | .5000 | 1.2290 |
| 29 | .5130 | .8925 |
| 30 | .5130 | .8925 |
| 31 | .8685 | .6880 |

^aDimensions are in inches.

TABLE III. - INTERNAL CONNECTOR DIMENSIONS^a

[Depth, 4 in.]

| Node | | Length | | Width | Node | | Length | | Width |
|------|------|--------|--------|--------|------|------|--------|--------|--------|
| I | J | I | J | | I | J | I | J | |
| 1 | 2 | 0.6430 | 0.7180 | 0.6720 | 15 | 16 | 0.5625 | 0.5625 | 0.812 |
| | 1002 | .2963 | ----- | 1.2860 | | 18 | .406 | .476 | 1.104 |
| | 1007 | .2963 | ----- | 1.3640 | | 1033 | .3016 | ----- | .9475 |
| 2 | 3 | 0.7180 | 0.5647 | 0.6720 | 16 | 17 | 0.406 | 0.476 | 1.104 |
| | 6 | .7180 | .5442 | .5470 | | 1035 | .3016 | ----- | 1.421 |
| | 12 | .6095 | .758 | .826 | 17 | 18 | 0.5397 | 0.5397 | 0.952 |
| | 1003 | .6095 | ----- | 1.436 | | 1015 | .476 | ----- | 1.0672 |
| | 1008 | .586 | ----- | .5883 | | 1036 | .3016 | ----- | 1.895 |
| | 1021 | .6095 | ----- | 1.131 | 18 | 19 | 0.5397 | 0.4782 | 0.952 |
| 3 | 6 | 0.336 | 0.547 | 1.114 | | 1014 | .476 | ----- | 1.0672 |
| | 1004 | .336 | ----- | 1.1372 | | 1037 | .400 | ----- | 3.191 |
| | 4 | .5647 | .636 | .672 | 19 | 20 | 0.4728 | 1.1115 | 0.562 |
| 4 | 7 | 0.336 | 0.547 | 1.254 | | 1013 | .476 | ----- | .9457 |
| | 1005 | .336 | ----- | 1.281 | | 1038 | .400 | ----- | 3.191 |
| | 5 | .636 | .636 | .672 | 20 | 1011 | 0.2087 | ----- | 1.102 |
| 5 | 1006 | 0.336 | ----- | 1.281 | | 1012 | .1897 | ----- | 2.223 |
| | 8 | .336 | 0.547 | 1.254 | | 1040 | .3062 | ----- | .9621 |
| 6 | 7 | 0.5442 | 0.613 | 1.094 | 21 | 22 | 0.245 | 0.245 | 1.250 |
| | 11 | .547 | .4845 | 1.063 | | 28 | .625 | .250 | .982 |
| | 12 | .5379 | .553 | .547 | | 1042 | .370 | ----- | 1.162 |
| | 1023 | .650 | ----- | 2.000 | 22 | 23 | 0.245 | 0.2725 | 1.250 |
| 7 | 8 | 0.613 | 0.613 | 1.094 | | 27 | .625 | .297 | .982 |
| | 10 | .547 | .4845 | 1.198 | | 1043 | .200 | ----- | 1.414 |
| | 1024 | .333 | ----- | .922 | 23 | 24 | 0.2725 | 0.2182 | 1.250 |
| 8 | 9 | 0.547 | 0.4845 | 1.198 | | 26 | .625 | .344 | 1.090 |
| | 1025 | .333 | ----- | .922 | | 1047 | .200 | ----- | 1.414 |
| 9 | 10 | 0.586 | 0.586 | 0.969 | | 1048 | .200 | ----- | 1.414 |
| | 16 | .4845 | .406 | 1.146 | | 1049 | .200 | ----- | 1.414 |
| | 1026 | .300 | ----- | 2.283 | 24 | 25 | 0.625 | 0.344 | 0.873 |
| | 1027 | .300 | ----- | 2.283 | | 1052 | .200 | ----- | 1.414 |
| 10 | 11 | 0.586 | 0.586 | 0.520 | | 1053 | .300 | ----- | 1.2566 |
| | 15 | .4845 | .406 | 1.146 | 25 | 26 | 0.5558 | 1.390 | 0.688 |
| | 1028 | .303 | ----- | 1.276 | | 1020 | .344 | ----- | 1.230 |
| 11 | 12 | 0.520 | 0.250 | 0.969 | | 1051 | .247 | ----- | 2.170 |
| | 14 | .4845 | .406 | 1.017 | 26 | 27 | 0.695 | 0.611 | 0.688 |
| | 1029 | .520 | ----- | 1.634 | | 1019 | .344 | ----- | 1.54 |
| 12 | 13 | 0.758 | 0.601 | 0.500 | | 1046 | .247 | ----- | 2.17 |
| | 1009 | .3315 | ----- | 1.560 | | 1050 | .247 | ----- | 1.626 |
| | 1022 | .413 | ----- | .663 | 27 | 28 | 0.611 | 0.589 | 0.500 |
| | 1054 | .333 | ----- | 2.042 | | 1018 | .297 | ----- | 1.344 |
| 13 | 14 | 0.325 | 0.4987 | 0.812 | | 1045 | .247 | ----- | 1.626 |
| | 19 | .5062 | .4836 | .390 | 28 | 1055 | .277 | ----- | .606 |
| | 20 | .601 | .281 | 1.225 | | 1017 | 0.250 | ----- | 1.277 |
| | 1010 | .400 | ----- | 1.450 | 29 | 30 | 0.4462 | 0.4462 | 0.556 |
| | 1030 | .250 | ----- | .7854 | | 1016 | .4462 | ----- | .580 |
| 14 | 15 | 0.4987 | 0.5625 | 0.812 | 30 | 1041 | 0.250 | ----- | 1.000 |
| | 19 | .406 | .476 | .978 | | 1001 | 0.344 | ----- | 0.851 |
| | 1031 | .3016 | ----- | .9475 | | | | | |
| | 1032 | .3016 | ----- | .9475 | | | | | |

^aAll dimensions are in inches.

~~CONFIDENTIAL~~

storage limited the fineness of the grid. Examples of the mechanics of nodal description are given in reference 4. Some of the more important considerations are presented as follows.

(1) The poison-plate thickness produced a node with little resistance to heat transfer; an extremely small time increment was required by TØSS for a stable solution. It was, therefore necessary to eliminate the poison-plate node from the model to conserve computer time.

(2) Several guide pins used for assembly were not considered as individual nodes but were considered as integral homogenous parts of other nodes because of the close mechanical fit provided for assembly purposes.

(3) A constant-thickness outer vessel was considered along with an adiabatic outer boundary. This allowed each station to be identical in plan and therefore simplified the input procedure. The actual pressure vessel had a varying thickness (see fig. 2).

(4) As mentioned previously, TØSS requires a connecting area and a connector length to define the heat-transfer effect of a surface node. Some difficulty, associated with the modeling of a circular passage within or on the physical boundaries of a large internal node, was experienced in specifying these dimensions. A typical situation is the surface node 1023 between the boundary node 2006 and the internal node 6 (fig. 14). As an example, a connecting area that is less than an area based on the perimeter of node 6 and greater than an area based on the circumference of the circular passage of boundary 2006 was needed in addition to an appropriate connector length to represent the heat-transfer network accurately.

(5) Because boundaries separated the pressure vessel and the inner reflector from the main reflector, the nodal representation of the cylinder and the inner reflector were simplified to one and two nodes, respectively. Heat-transfer calculations suffered little from this modeling; however, the flow calculations were affected.

In addition to the problem areas just mentioned, other problems were apparent in modeling the reflector system. Some of these will be discussed further in the next section.

RESULTS AND DISCUSSION

Runs Analyzed

Many cold-flow runs have been made in the facility described, each with specific and slightly different objectives. Runs 11, 19, and 24 were selected to be compared with the analytical results in this report. Table IV is a summary of the major test parameters for these runs. Run 24 resulted in the highest flow rates and pressures; those from

TABLE IV. - IMPORTANT TEST PARAMETERS

| Parameter | Run | | |
|--|------|------|-------|
| | 11 | 19 | 24 |
| Tank pressure, psia | 50 | 35 | 35 |
| Time of cooldown before bootstrapping, sec | 10 | 5 | 0 |
| Run time (considered for comparison with predictions), sec | 18 | 25 | 13 |
| Flowrate at end of run time, lb/sec | 15.4 | 13.4 | 29.8 |
| Reflector inlet pressure at end of run time, psia | 68 | 53.8 | 112.2 |
| Reflector inlet quality at end of run time | 0 | 0.1 | 0 |
| Reflector outlet plenum fluid temperature at end of run time, °R | 240 | 220 | 200 |

runs 11 and 19 were considerably lower. For run 11, 96 experimental measurements of different reflector parameters were made. For runs 19 and 24, 52 measurements were made. Run 11 is compared in detail with the results of the prediction program; however, some typical results from runs 19 and 24 are presented, for comparison.

Experimental Input Data

As mentioned earlier, reflector-inlet fluid properties (as a function of time) and the initial reflector material temperature distribution are used as input data to the prediction program.

Flow rate. - For runs 11, 19, and 24 in figure 15 are shown (1) the tank-exit flowmeter flow rate (flow rate entering the system), (2) the calculated (see ref. 6 for details of the calculation from experimental data) nozzle flow rate (flow rate leaving the system) and (3) the calculated reflector-inlet flow rate which is the input to the prediction program. The method used to calculate the reflector inlet flow rate is presented in detail in reference 8. Briefly, the method is outlined as follows:

(1) The calculated nozzle flow rate is used as the reflector inlet flow rate until two-phase flow reaches the reflector inlet. Storage of gaseous hydrogen between the reflector inlet and nozzle throat is assumed to be negligible when the flow is all gas.

(2) The tank-exit flowmeter flow rate is used as the reflector-inlet flow rate after saturated liquid is indicated at the reflector inlet. Storage of liquid hydrogen as a function of time between the reflector inlet and the tank exit is assumed to be negligible

when the flow is all liquid.

(3) A linear interpolation scheme is used to obtain values of reflector-inlet flow rate as a function of time, when two-phase flow is indicated at the reflector inlet. The solid line in figure 15 indicates the reflector-inlet flow rate determined by this method.

Since the RAFF portion of the prediction program uses a time increment of about 1 second, the average value of flow rate (as well as enthalpy and pressure) over the entire time increment must be supplied as input data. Also, flow rate is assumed to be invariant with length.

Inlet pressure. - The experimental reflector-inlet pressure as a function of time is shown in figure 16. Two measurements were recorded for these runs, RP-140 at an angular position θ equals 30° and RP-141 at θ equals 150° (see fig. 8). The installation of the static pressure taps for RP-140 and RP-141 consisted of drilling a hole through the pressure vessel at $Z = 53$ inches, tapping the hole, and connecting the transducer to the tapped hole. Calculations have shown that a substantial pressure gradient exists from the nozzle-coolant tube outlet, across the reflector bracket (see fig. 8), to the outer reflector-coolant passages. The inlet pressure used in the prediction program is indicated by the solid line in figure 16 and is assumed to be the same for each reflector-coolant passage. Obviously, an error is introduced into the calculations by this assumption; this error is discussed further in the section Material temperatures.

Enthalpy. - A method of calculating the enthalpy at the various interfaces within the system is also presented in reference 8 and is briefly described as follows:

(1) The state of the fluid at the pump main discharge valve (see fig. 1) is taken to be saturated liquid at time zero. After time zero, the enthalpy is obtained as a function of pressure and temperature measured at that point.

(2) The change in enthalpy at any point in the system and for a certain time increment is obtained from

$$\Delta H = \frac{Q}{\dot{w}}$$

where Q is the heat added to the hydrogen from the warm material in that part of the system. The heat flux Q is calculated from the rate of temperature change with time of the many thermocouples in the system.

$$Q = mC_p \frac{\Delta T}{\Delta \tau}$$

The flow rate \dot{w} was calculated by using the method outlined earlier in the section Flow rate. (See ref. 8 for the details of these calculations.)

[REDACTED]

The enthalpy of the fluid at the nozzle-coolant-tube outlet was used as the inlet enthalpy for all the reflector-coolant passages and is shown in figure 17. As was the case with the reflector-inlet pressure, a substantial gradient in inlet enthalpy is also known to exist; the large mass of material in the pressure vessel, which contains the reflector inlet plenum (fig. 8), is a significant source of heat flowing to the fluid as the hydrogen makes its way from the nozzle-coolant tubes into the various reflector-coolant passages. Thus, the assumption that a constant inlet enthalpy exists for all the reflector passages obviously introduces some error in the analysis; this error will also be discussed in the section Material temperatures.

Initial material temperature. - Since the system downstream of the pump main discharge valve was at ambient temperature prior to the runs, the initial material temperatures used in the reflector prediction program were obtained by observing the temperature output from the many thermocouples within the reflector prior to the opening of the main valve. An average value was used for the entire reflector.

Comparison of Experimental and Predicted Results

Exit pressure. - A comparison of experimental and predicted reflector-exit-plenum pressure is presented in figure 18 for runs 11, 19, and 24. The predicted results agree very well with the experimental data for run 11. For runs 19 and 24, the predicted pressures tend to be lower than the experimental data; a maximum difference of about 12 percent is noted near the end of run 19.

Pressure drop. - Figure 19 compares predicted and experimental reflector pressure drop as a function of time for runs 11, 19, and 24. Rather severe fluctuations are noted in the predicted pressure drop curves in this figure. Figure 20 presents a comparison of the rate of change of flow rate and inlet pressure with time plotted as a function of time. It is seen that the irregularities in the predicted reflector pressure-drop data in figure 19(a) correspond to similar irregularities in the data presented in figure 20. Thus, the irregularities in the predicted pressure-drop results (figs 19) correspond to the variation in the input data supplied to the program. Therefore, since the input data supplied was an average value over the time increment considered, a shorter time increment would probably have smoothed some of the irregularities in figure 19.

Exit fluid temperature. - As shown in figure 11, reflector exit fluid-temperature measurements were made in the reflector exit plenum ($Z = -3$ in.) and just at the outlet of several of the passages ($Z = -0.25$ in.).

Plenum: Figure 21 compares predicted and experimental temperatures in the reflector-outlet plenum. The experimental measurements, RR-619, RR-622, and RR-624 for run 11 and RR-619, RT-622, and RR-624 for runs 19 and 24, were made at

[REDACTED]

angular positions $\theta = 45^\circ$, 115° , and 235° , respectively. Differences in the experimental measurements are as high as 50° R for run 11, 46° R for run 19, and 65° R for run 24.

The predicted results follow similar trends for each of the three runs. During the first few seconds of each run the predicted exit plenum temperature diverges from the experimental temperatures. For the next few seconds of each run, the predicted temperatures are about 6 percent below, but approximately parallel to the experimental results. Finally, from about the midpoint to the end of each run, the predicted plenum temperatures lie generally between the extremes of the experimental measurements.

The fluid at the reflector inlet is all gas for about 4 seconds for run 11, 5.6 seconds for run 19, and 4.5 seconds for run 24. In each case, this time corresponds to about the time when the divergence of the predicted temperatures from the experimental temperatures ends. Thus, it appears that, while the fluid is all gas, the total predicted heat transfer to the gas is low. In reference 1 (the single-tube study in which the geometry of the tube was well defined), the predicted and experimental exit-fluid-temperature results agreed very well for an all-gas run. Thus, it appears that the problem lies not with the method used but rather in the model used to represent the complex reflector sector. In other words, it appears that the arbitrary connector lengths and widths used (connecting the surface nodes with their respective internal temperature nodes) were not properly chosen to provide the correct heat-transfer rate.

Carrying the preceding line of reasoning one step further (i.e., to the portions of the runs in which two-phase flow was indicated at the reflector inlet and at least part way through the reflector passages), it appears that the predicted rate of heat transfer to the two-phase hydrogen may be too high. Then, as time increases and the two-phase - gas interface moves up in the reflector passages, the low rate of heat transfer to the gaseous hydrogen in the passage is overcome by the high rate to the two-phase hydrogen; the result at the reflector exit is reasonable agreement between the predicted and experimental fluid temperatures.

Reference 1 also considered two-phase flow through the single tube. The predicted exit fluid temperatures for these runs were 5 to 10 percent lower than the experimental data, however, indicating that the heat transferred to the two-phase part of the flow was too low. Thus, an anomaly exists between the data presented in reference 1 and the trends indicated in figure 2. The reason for this inconsistency will be revealed as the remaining results are discussed.

Passage: A comparison of the predicted and experimental results at several passage exits are shown in figure 22. Figures 22(a), (b), and (c) show the results at the exit of circular passages G, E, and C (see fig. 11), respectively. The agreement between the predicted and experimental results are within about 20 percent. Figures 22(d), (e), and (f), on the other hand, show the results at the exit of the three noncircular passages

[REDACTED]

D, B, and F, respectively (see fig. 11). Large differences are observed between the predicted and experimental temperatures for slots B and F. Slot B is the restricted passage between the graphite inner-reflector and the aluminum outer-reflector segment. Slot F is between the outer-reflector segment and the pressure-vessel wall. The reason for these wide discrepancies is not apparent from the results presented to this point; this will be explained in more detail in the section Material temperatures.

Axial fluid temperature. - As mentioned in the section Instrumentation, three platinum-film resistance temperature probes were installed on the simulated poison plate of one of the control drums to measure fluid temperature within the control drum slot. Figure 23 compares the results of these probes with predicted values as a function of time for run 11. (These measurements were not recorded for runs 19 and 24). A problem is indicated on the high end of the temperature scale for the resistance probes; the measured temperatures indicated about 545° R while the ambient temperature was only about 522° R. The reason for this discrepancy is not known. The accuracy on the low end of the scale appears to be good, however, since all of the measurements approach liquid-hydrogen temperature, as expected.

The predicted results near the reflector inlet ($Z = 46$ in.) and near the middle of the reflector ($Z = 28$ in.) agree reasonably well with the experimental data. Discontinuities are observed in the predicted results, however, when two-phase flow is present in the passage. Near the passage exit ($Z = 2$ in), the predicted results are considerably higher than the experimental data. These results are in general agreement with the results presented in figure 22(d) for the fluid temperature at the exit of this passage.

The only conclusion that can be reached regarding the use of this type of device to measure fluid temperatures is that more work is required on the calibration. No conclusions can be made as to response or accuracy of the instruments over most of the range.

Material temperatures. - Figure 24 shows a plot of predicted isothermal lines in the 15° section of the reflector at time equal to 18 seconds of run 11 for lengths approximately 2, 22, and 50 inches from the reflector inlet. Available experimental measurements are also shown in this figure, and several important points should be recognized. First, consider only the experimental temperatures shown. At each axial position, the pressure vessel remains relatively warm. Within the outer reflector, the temperatures range from relatively high, near the pressure vessel, to quite low, near the graphite inner-reflector cylinder. The coldest part of the reflector is obviously the graphite inner-reflector cylinder.

Thus, it appears from figure 24 that the experimental reflector-assembly (excluding the control drum) temperature is strongly a function of radial position. The experimental temperature within the control drum appears to be warmest near the poison-plate slot and coolest on the opposite side of the drum. It should also be noted that the

[REDACTED]

reflector bracket (see fig. 8) was designed to distribute the flow at the reflector inlet under full-power operation and under these conditions should yield a reasonably uniform temperature distribution at the reflector outlet. Under full-power operation, of course, the heat generation rate per unit volume would be some inverse function of the radial position in the reflector. Thus, it appears that the experimental temperatures recorded for this run are reasonable. (Similar results were obtained for runs 12 and 24.)

Next, consider the predicted isothermal lines in figure 24. The predicted temperatures in the pressure vessel are lower than the experimental temperatures; the predicted temperatures in the graphite inner cylinder are considerably higher than experimental. The predicted temperatures within the outer-reflector segment tend to be more a function of angular position than of radius. Several problems are obvious from these trends. First, and probably most important, the reflector-inlet plenum conditions (pressure and enthalpy) were assumed to be the same for each passage. Thus, the flow-rate distribution predicted by the program is controlled; the pressure drops across each passage are equal. In the actual reflector, however, a sizeable pressure gradient exists from the nozzle-tube outlet to the pressure-vessel inlet annulus (see fig. 8). As a result, the pressure drops across the passages in the experiment are obviously not equal.

This pressure maldistribution at the reflector inlet explains some of the poor predictions in figure 24. The actual pressure at the inlet of the graphite inner-reflector cylinder passages and slot is higher than the pressure used as input to the prediction program; the experimental inlet pressure measurement was made through the pressure-vessel wall. As a result, the flow rates through these passages are much higher than predicted, which explains the very high predicted temperatures in the graphite reflector cylinder; the higher flows of hydrogen cool the material faster than predicted. Similarly, the flow rates for the other passages in the reflector are lower than the values used in the calculations; hence, the increase in experimental material temperature from the graphite cylinder to the outer reflector is expected.

A similar situation exists as a result of assuming that the inlet enthalpy is constant. The inlet enthalpy used in the prediction program corresponds to the fluid state at the nozzle tube outlet; whereas, the actual inlet enthalpy is known to be a function of the passage location. Reference 1 showed that pressure drop was strongly a function of inlet enthalpy. As the actual enthalpy varied from passage to passage, the actual pressure drop would tend to vary in the same way. The pressure drop is fixed, however, and the result is a corresponding redistribution of flow rate; the actual flow rate distribution would indicate lower flow in the passages with the higher inlet enthalpy. Thus, assuming both inlet pressure and enthalpy constant at each passage inlet caused the predicted flow rate to be low in the graphite reflector cylinder and high in the other passages. Obviously, to determine the flow rate and inlet enthalpy for each passage experimentally would have required an unrealistic number of additional measurements (fluid tempera-

[REDACTED]

atures and pressures, pressure differences, quality indicators, etc.)

In the pressure-vessel wall, the experimental temperatures are higher than predicted probably because, the outer surface of the prediction model is assumed to be adiabatic. In reality, this surface is exposed to ambient conditions, and some heat enters through this boundary that maintains the temperature higher than predicted.

Another problem that was mentioned briefly in the ANALYTICAL PROCEDURE section may also be contributing to the unsatisfactory results presented in figure 24. Consider boundary node 2033, for example, in figure 14. The TØSS part of the prediction program uses the boundary temperature and heat-transfer coefficient (calculated in RAFF) to calculate wall and material temperature changes over some time interval (usually about 1 sec in this study). At the end of the time interval, RAFF calculates new fluid properties and heat-transfer coefficients based on the updated wall temperatures. However, RAFF uses for its calculations only one wall temperature for each boundary temperature; in the cases where there is more than one wall temperature for a boundary temperature, an arithmetic average wall temperature is used. The problem is apparent on boundary node 2033. Temperatures of surface nodes 1012, 1013, 1014, 1015, and 1016 (see fig. 14) are averaged to obtain the wall temperature for RAFF that will determine the fluid temperatures and heat-transfer coefficient to be used on the next time increment. Figure 24(a) shows that the temperature of node 1016 is lower than the other four nodes. The resulting average wall temperature will be too high for node 1016, and the heat transfer from node 1016 to 2033 for the next time increment can be expected to be too low. Thus, the predicted graphite cylinder temperatures can be expected to be high. A similar problem exists on boundary node 2030, and to a lesser degree, on 2031 and 2032. A better method of calculating average wall temperatures around these passages is obviously required.

This wall-temperature weighting problem explains, at least in part, the large differences between the predicted and experimental fluid temperatures at the exit of slot B (see fig. 22(e). Around slot F, however, figure 22(f) shows that the wall temperature of the pressure vessel is generally between the extremes in temperature of the adjacent outer-reflector wall; the averaging technique used probably yields reasonably results for this slot. Similarly, the surface node temperatures around the slots 2031 and 2032 were close enough so that the averaging presented no apparent problem.

Axial material temperature distribution. - Another serious problem area in the prediction program, the axial material temperature distribution, is presented in figure 25 for several locations within the reflector for run 11. The thermocouple locations are shown schematically in figure 10 and the predicted temperatures in figure 25 represent the temperature of the node in which the thermocouple was installed. For example, in figure 25(a) nodes 31, 62, and 93 (see fig. 14) were used to compare with the thermocouples in location A (fig. 10). Figure 25(a) compares pressure-vessel temperatures

[REDACTED]

and figures 25(b) to (e) compare temperatures at locations B to E, respectively. In the outer-reflector segment, figure 25(f) shows graphite reflector cylinder temperatures (location F), and figures 25(g) to (i) present material temperatures within the control drum.

It is expected from the previous discussion of flow maldistribution that the predicted temperatures near the pressure vessel should be lower than experimental temperatures, and that the predicted temperatures in the graphite cylinder should be generally higher than experimental. This general trend is exhibited in figures 25(a), (b), (e), and (f), Figures 25(c) and (d), near the middle of the outer reflector, and figures 25(g) to (i), within the control drum, are not expected to be generally high or low.

The unusual shape of the predicted material temperature curves shown in these figures indicates a problem area, however. The humps and wiggles that progress downstream as time increases are caused by a transition from two-phase flow to gas flow. The change in predicted heat-transfer coefficient from the two-phase correlation to the all-gas correlation is not smooth but actually exhibits a discontinuity at the point of change. This abrupt transition probably causes the unexpected temperature profiles.

The experimental temperatures shown in figure 25, for the most part, increased with distance from the reflector entrance, as expected. In figure 25(e) where the material temperature changed very rapidly, however, a hump is seen in the experimental data similar to the hump seen in the predicted data. Reference 1 also presented material-temperature data that appeared to show the effect of transition from two-phase to gas flow. There are not enough data from these runs, however, to reach any strong conclusions. It is obvious that more work is required in the transition region.

Another unexpected result shown in figure 25 is the negative slope near the reflector inlet of the curves showing temperature as a function of length for times near the end of the run (i. e., two-phase flow in the passages). The experimental data in this area exhibit a steep positive slope. Thus, contrary to the results indicated in figure 21, the predicted heat-transfer to the two-phase fluid is too low. The heat transfer coefficients in this region is low because of the low fluid quality.

CONCLUDING REMARKS

A comparison of predicted and experimental exit plenum pressures indicated very good results; a maximum difference of about 12 percent was noted. A comparison of reflector pressure drop, predicted and experimental, showed reasonable agreement (within 20 percent, for the most part). Rather severe fluctuations in the predicted results were noted. These fluctuations were consistent with the inlet flow rate and pressure used as input to the prediction program; improved prediction would probably

[REDACTED]

result if shorter time increments had been used.

Reflector-exit plenum fluid temperatures were also compared, and the results were generally good (within 6 percent or 31° R). Similarly, predicted fluid temperatures at the exit of several circular passages were within about 15 percent of the experimental data. Predicted fluid temperatures at the exit of several annuli, however, were far from the experimental data. These differences were apparently caused by the method used to obtain the average wall temperature around these annuli in the fluid calculations and by the assumption that the pressure and enthalpy were the same at the entrance to all passages. It was shown that this assumption caused too much predicted flow in the outer-reflector passages and too little predicted flow in the reflector-cylinder passages.

As a result of this flow distribution problem the predicted material temperatures did not agree well with the experimental temperatures. The predicted temperatures were generally high near the inner reflector and too low in the outer reflector and pressure vessel.

A comparison of predicted and experimental axial temperature distributions also indicated poor agreement; more heat-transfer investigations are required in the areas of two-phase flow and two-phase to gas transition.

Lewis Research Center,

National Aeronautics and Space Administration,


Cleveland, Ohio, March 29, 1967,

122-29-01-03-22.

APPENDIX A

SYMBOLS

| | | | |
|----------------|---|-----------------|---|
| A | hydraulic area, ft ² | Q | heat flux, Btu/sec |
| A _s | passage increment surface area, ft | R | ratio fraction |
| B _i | exponent defined in eq. (B19) | Re | Reynolds number, GD/μ |
| C | C _p ρV, Btu/°R | T | temperature, °R |
| C _p | specific heat, Btu/(lb)(°R) | u | temperature as function of time |
| D | hydraulic diameter, ft | \dot{w} | mass flow rate, lb/sec |
| f _n | friction coefficient | X | quality |
| G | specific flow rate, \dot{w}/A , lb/(sec)(ft ²) | x | dimension |
| g _c | gravitational constant, ft/sec ² | Y | thermal admittance, Btu/(sec)(°R) |
| H | enthalpy, Btu/lb | y | dimension |
| h | heat-transfer coefficient, Btu/(sec)(ft ²)(°R) | Z | axial distance from top of reflector, in. |
| h _v | velocity head loss coefficient | z | dimension |
| i | passage number index | α | reflector segment centerline angular position, deg |
| J | conversion factor, ft-lb/Btu | θ | angular position in reflector, deg |
| K | $0.5 \left(\frac{Re}{3000} \right)^{0.077} - 0.070$ (see ref. 12) | μ | viscosity, lb/(ft)(sec) |
| k | thermal conductivity, Btu/(ft)(sec)(°R) | ρ | density, lb/ft ³ |
| L | distance from reflector inlet plane, in. | τ | time, sec |
| m | mass, lb | X _{tt} | Martinelli parameter |
| N | total number of passages (range of i) | Subscripts: | |
| P | pressure, psia | av | average |
| Pr | Prandtl number, Cpμ/k | b | bulk |
| | | ex | exit |
| | | f | film |
| | | fr | friction |
| | | g | gas |



| | | | |
|-----|---|---------|---|
| i | passage axial increment number index | p | index of neighbor nodes of inter- nal node q |
| in | inlet | q | internal node (see ref. eq. (4)) |
| k | iteration number | res | restriction |
| l | liquid | tot | total |
| m | momentum | w | wall |
| ma | maximum | τ | time |
| min | minimum | 2ϕ | two phase |
| n | last increment of passage i | | |

APPENDIX B

FLUID-FLOW ANALYSIS

Reflector Analysis Fluid Flow (RAFF)

An analytical procedure was formulated for calculating fluid temperatures and pressure drops of hydrogen fluid in a multipassage reflector system due to quasi-steady-state material temperatures. A computer program (RAFF) was written, based on this formulation, in FORTRAN IV source language. A subroutine STATE(J) is used by RAFF to calculate the hydrogen state variables (ref. 9).

RAFF requires the following parameters and geometry data as input:

(1) Inlet fluid properties:

(a) Enthalpy H_{in} at inlet conditions as a function of time

(b) Inlet pressure (P_{in}) as a function of time

(c) Composition of hydrogen in terms of percent ortho

(2) Total inlet flow rate (\dot{w}_{tot}) as a function of time

(3) Geometry

(a) Diameters of all the circular passages

(b) Lengths and widths of slotted passages

(c) Hydraulic area A_{res} and head loss coefficient h_v of any restrictive passage

(4) An average initial wall temperature T_w for each passage increment

Subsequent wall temperatures are obtained from TØSS.

Calculational Procedure

The computer code RAFF is concerned with the calculation of flow parameters by assuming a steady-state condition to exist for an instant in time. The formulation that follows was based on mean values with respect to succeeding time increments of enthalpy, inlet pressure, and inlet-total flow rate of the fluid. Convective heat transfer based on turbulent fluid flow was assumed.

Entrance conditions. - For a given total flow rate \dot{w}_{tot} , the distribution among all the passages was determined initially by

$$\dot{w}_i = R_i \dot{w}_{tot} \quad (B1)$$

where R_i is the ratio of the flow rate through passage i to the total flow rate \dot{w}_{tot} . This ratio must be supplied as input data for the first time increment. The value of R_i

resulting from the flow balancing for time τ is used as the initial estimate of R_i for time

$$\tau + \Delta\tau$$

The stagnation inlet-plenum total pressure was converted to a static pressure just inside a passage by the following expression that includes entrance losses:

$$P_{j=1} = P_{in} - (1 - K) \frac{G_i^2}{2g_c \rho_{in} \times 144} \quad (B2)$$

The enthalpy at the entrance to each passage was obtained by assuming constant total enthalpy across the entrance

$$H_{j=1} = H_{in} - \frac{G_i^2}{2g_c J \rho_{in}^2} \quad (B3)$$

Heat-transfer equations. - Each passage was divided into j axial increments ΔL inches long. An average wall temperature $T_{w,j}$ was assumed to exist over the increment length. The average value of the heat flux Q_j was obtained from an iteration process to determine the average bulk temperature of the fluid $T_{b,av}$, which is also a function of Q_j . The inlet state of the fluid to an increment supplies the initial estimate of the fluid bulk temperature $T_{b,j}$. The iteration procedure for an increment begins with the calculation of the heat flux:

$$Q_j = hA_s(T_{w,j} - T_{b,av}) \quad (B4)$$

The convective heat-transfer coefficient h for turbulent fluid flow for a fluid in the gas region ($x \geq 0.90$) is based on average bulk properties:

$$h_g = 0.021 \frac{k}{D} Re_b^{0.8} Pr_b^{0.4} \left(\frac{T_w}{T_b} \right)_j^{-0.575} \quad (1)$$

For fluid in the two-phase region ($0.05 < x < 0.90$), the heat-transfer coefficient is based on average film properties,

$$h_{2\phi} = \frac{0.023 \frac{k}{D} Re_f^{0.8} Pr_f^{0.4}}{0.611 + 1.93 \chi_{tt}} \quad (2)$$

where the Martinelli parameter is used and defined by

$$\chi_{tt} = \left(\frac{1-x}{x} \right)^{0.9} \left(\frac{\mu_l}{\mu_g} \right)^{0.1} \left(\frac{\rho_g}{\rho_l} \right)^{0.5} \quad (B5)$$

A simplified form of the energy equation is used to obtain the exit enthalpy of increment j based on the assumption of a low Mach number so that the static enthalpy is approximately equal to the total enthalpy

$$H_{j+1} = H_j + \frac{Q_j}{w_i} \quad (B6)$$

Pressure-drop equations. - The pressure drop across the increment is calculated in order to provide a state variable P in addition to enthalpy H_{j+1} (eq. (B6)) to arrive at a bulk temperature at the end of increment j . The pressure at station $j+1$ is obtained from

$$P_{j+1} = P_j - \Delta P_{fr} - \Delta P_m - \Delta P_{res} \quad (B7)$$

The pressure drop due to friction is obtained from

$$\Delta P_{fr} = 4f_n \frac{\Delta L}{D} \frac{G_i^2}{2g_c \rho_{av} \times 144} \quad (B8)$$

where

$$\rho_{av} = \frac{\rho_j + \rho_{j+1}}{2} \quad (B9)$$

and f_n is obtained by iteration from the expression (ref. 13)

$$f_n = \frac{T_{b,av}}{T_f \left(4.0 \log \text{Re}_f \frac{\rho_f}{\rho_b} \sqrt{f_n \frac{T_f}{T_b}} - 0.4 \right)^2} \quad (\text{B10})$$

The pressure drop due to momentum was obtained from

$$\Delta P_m = \frac{G_i^2}{g_c \times 144} \left(\frac{1}{\rho_{j+1}} - \frac{1}{\rho_j} \right) \quad (\text{B11})$$

If a restriction is present in the passage, the following pressure drop is calculated

$$\Delta P_{res} = h_v \left(\frac{A_i}{A_{res}} \right)^2 \frac{G_i^2}{2g_c \rho_{av} \times 144} \quad (\text{B12})$$

Using current values of H_{j+1} and P_{j+1} (eqs. (B6) and (B7)) gives a current value of $T_{b,j+1}$ from the hydrogen properties subroutine STATE(J). This procedure, starting with equation (B4), is repeated until successive values of Q_j are within a tolerance of 2 percent. Average temperatures are obtained from

$$T_{b,av} = \frac{T_{b,j+1} + T_{b,j}}{2} \quad (\text{B13})$$

$$T_{f,av} = \frac{T_{w,j} + T_{b,av}}{2} \quad (\text{B14})$$

Exit conditions. - After the last station n of each passage has been completed, an exit plenum total pressure is calculated from (ref. 13)

$$P_{ex} = P_n - \frac{0.944 G_i^2}{2g_c \rho_n \times 144} + \frac{\rho_n V_n^2}{2g_c \times 144} \quad (\text{B15})$$

The total pressure drop across a passage i is

$$\Delta P_i = P_{in} - P_{ex} \quad (\text{B16})$$

CONFIDENTIAL

The overall convergence criteria adopted to end the RAFF calculations for a time increment was based on the exit plenum pressure vector P_{ex} . Each element of the vector, formed from the final values of $P_{ex,i}$ of equations (B15), was required to be essentially identical; this is accomplished by requiring the relative error between the maximum and minimum values of the elements to be within a predetermined tolerance, again consistent with the input data.

Flow-Rate Adjustments

To accomplish this pressure balancing, the flow rate \dot{w} was adjusted in two ways.

Flow-rate reduction. - Whenever either pressure P_{j+1} or P_{ex} was computed negative for all passages, the current flow rate \dot{w}_{in} was arbitrarily reduced by 2 percent. The calculations were restarted by using all original input data except for the reduced flow rate.

Flow-rate redistribution. - Two conditions required a redistribution of \dot{w}_{tot} among the passages: (1) The overall convergence criteria was not satisfied and (2) negative pressures were calculated at the exit of some (but not all) of the passages. The total flow rate was redistributed among all the passages by the following equations


$$\dot{w}_{i,k+1} = \dot{w}_{i,k} \left(\frac{\Delta P_{k+1,av}}{\Delta P_k} \right)^{B_i} \quad (B17)$$

where

$$\Delta P_{i,k+1,av} = \left[\frac{\dot{w}_{i,k}}{\sum_{i=1}^N \dot{w}_k / (\overline{\Delta P_k})_i} \right]^2 \quad (B18)$$

and

CONFIDENTIAL




$$B_i = \frac{\ln \left(\frac{\dot{w}_{k+1}}{\dot{w}_k} \right)_i}{\ln \left(\frac{\Delta P_{k+1}}{\Delta P_k} \right)_i} \quad (B19)$$

Since two values of \dot{w} and ΔP are required to calculate \dot{w}_{k+1} , B_i was assumed equal to 0.5 in equation (B17) for the second iteration pass. Details of this flow-balancing procedure are given in reference 6.

REFERENCES

1. Chenoweth, Francis C.; Watt, James J.; and Sprague, Earl L.: Transient Chillover of a Single Thick-walled tube by Liquid and Gaseous Hydrogen. Estimated Publication, approximately Nov. 1966.
2. Anon.: Nuclear Engine Transient Analysis Program. Rep. No. RN-DR-0068, Vol. I, Aerojet-General Corp., 1965.
3. Lee, A. Y.: A Program for Steady State Fluid Flow and Heat Conduction Coupled Calculations of Heat Generating Solids Cooled by Parallel Channels - Using MCAP and TØSS Codes. Rep. No. WANL-TME-967, Westinghouse Electric Corp., Astronuclear Lab., Oct. 1964.
4. Bagwell, David: TØSS - An IBM-7090 Code for Computing Transient or Steady State Temperature Distributions. Rept. No. K-1494, Oak Ridge Gaseous Diffusion Plant, Dec. 1, 1961.
5. Rostafinski, Wojciech; Rudey, Richard A.; Lacy, Donald D.; and Lillis, Patrick R.: Performance Characteristics of an Axial-Flow Liquid-Hydrogen Pump During Startup. NASA TM X-1213, 1966.
6. Clark, John S.: Analytical and Experimental Study of Startup Characteristics of a Full-Scale Unfueled Nuclear-Rocket-Core Assembly. NASA TM X-1231, 1966.
7. Turney, George; and Cox, Eileen: Cooldown Characteristics of Regenerative Nozzle Used in Full-Scale, Cold-Flow, Nuclear Rocket Test Facility. NASA TND-3931, 1966.
8. Straight, David M.; Biesiadny, Thomas J.; Pierce, John G.; and Metger, George W.: Component Flow and Fluid Properties During Cold-Flow Experiments in a Nuclear Rocket System. NASA TM X-1366, 1966.
9. Harry, David P., III: Formulation and Digital Coding of Approximate Hydrogen Properties for Application to Heat-Transfer and Fluid-Flow Computations. NASA TN D-1664, 1963.
10. Kreith, Frank: Principles of Heat Transfer. 2nd ed. International Textbook Co., 1965.
11. Moynihan, D. C., Jr.: A Survey of Heat Transfer and Hydrodynamic Problems Associated with Propulsion Reactors. Rept. No. SM-44891, Douglas Aircraft Co., Inc., Aug. 1964.
12. Hendricks, R. C.; Graham, R. W.; Hsu, Y. Y.; and Friedman, R.: Experimental Heat Transfer and Pressure Drop of Liquid Hydrogen Flowing through a Heated Tube. NASA TN D-765, 1961.

- 
13. Cavicchi, R. H. ; Ellerbrock, H. H. ; Hall, E. W. ; Heppler, H. J. ; Livingood, J. N. B. ; and Schwenk, F. C. : Design Analysis of a Subsonic Nuclear-Powered Logistic Airplane with Helium-Cooled Reactor. NASA TM X-28, 1959.

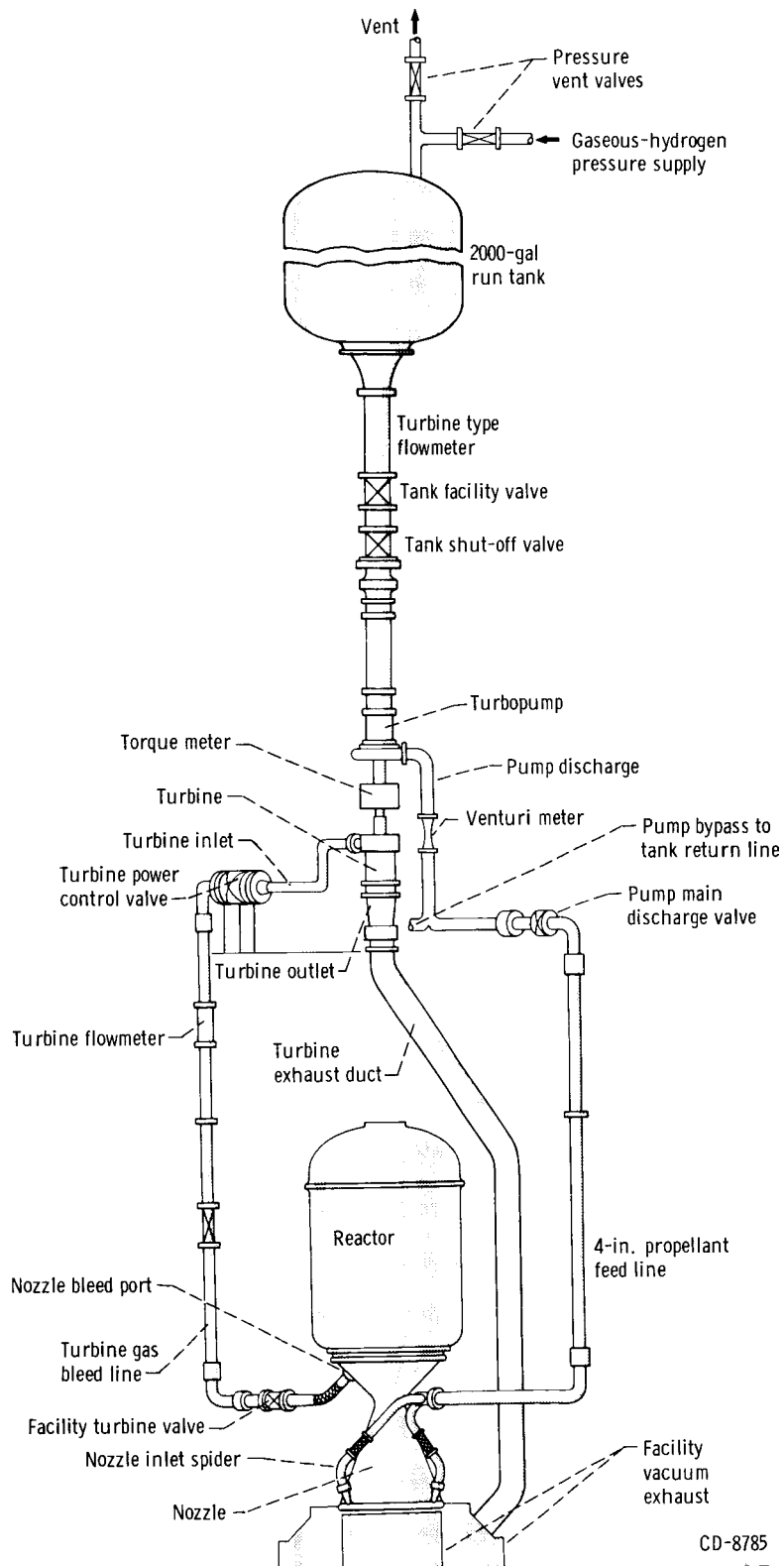


Figure 1. - Schematic drawing of nuclear-rocket cold-flow experiment.

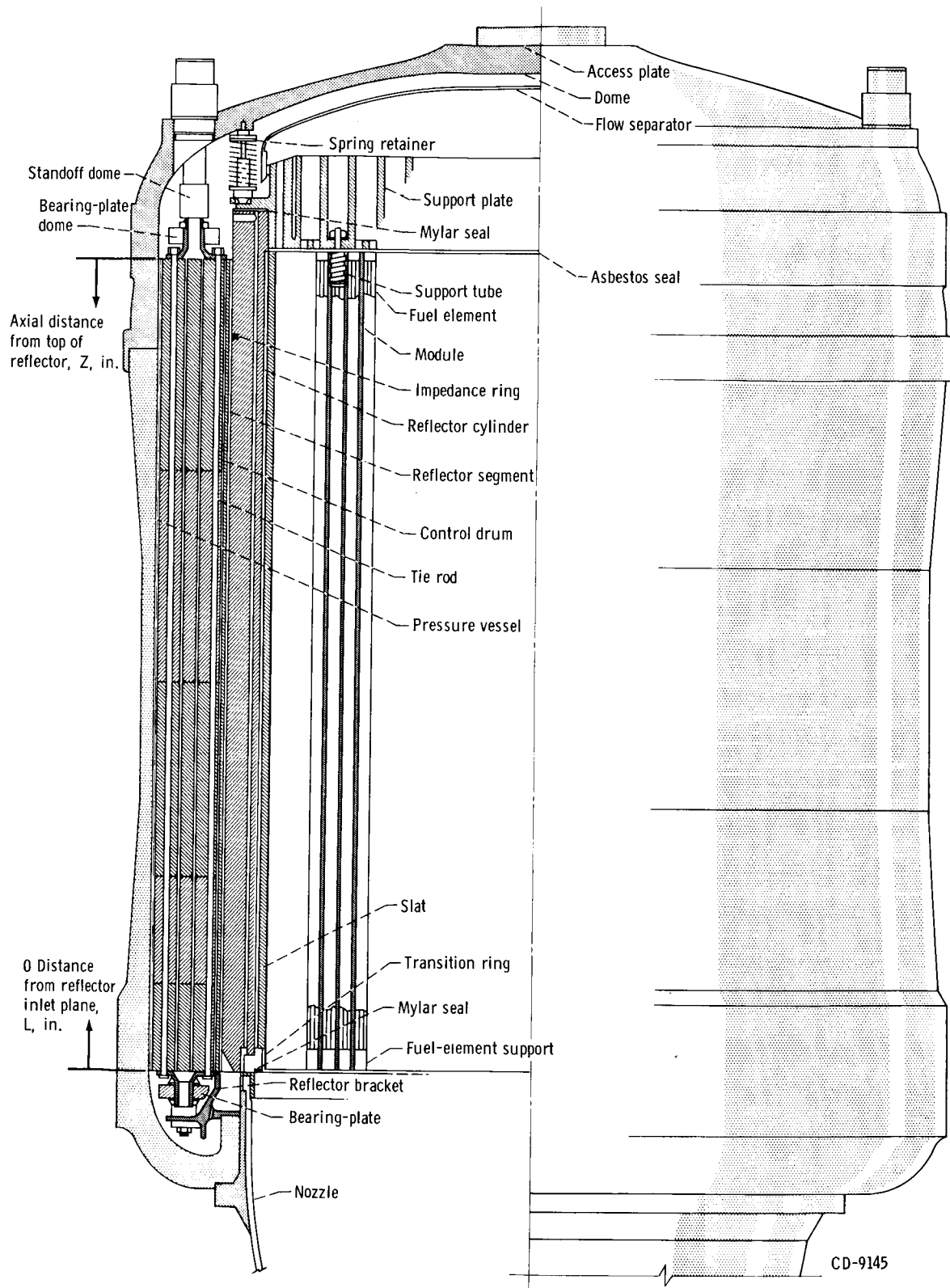
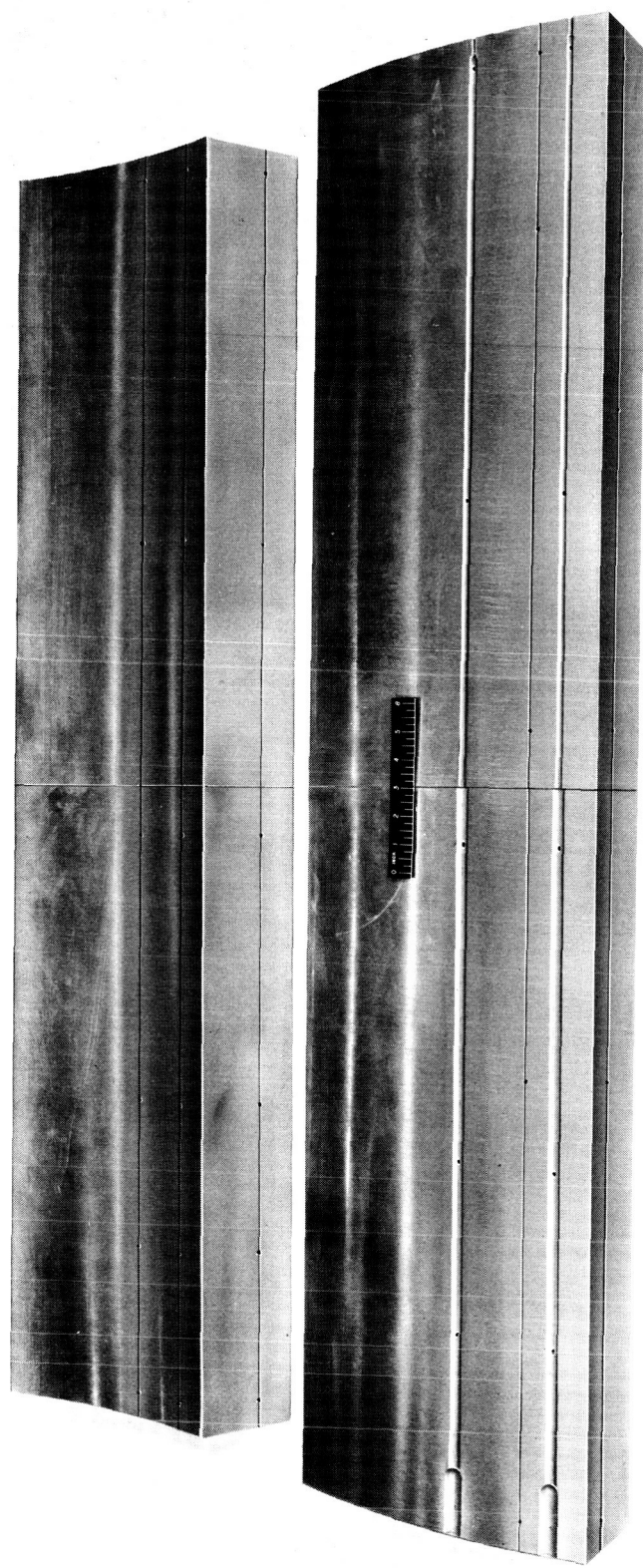
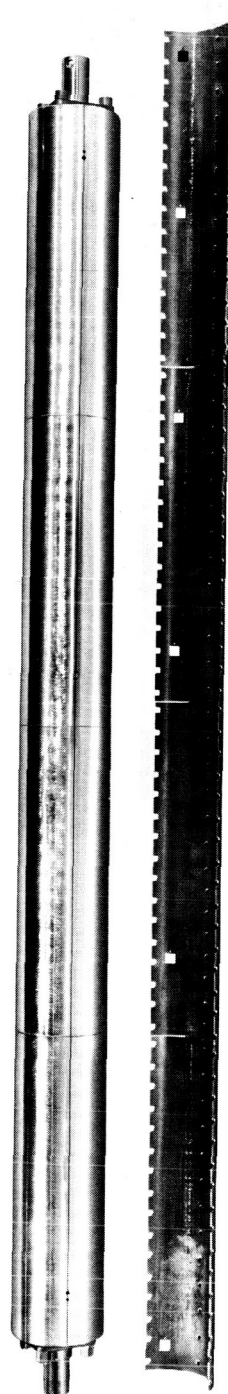


Figure 2. - Schematic diagram of reactor.



C-62537

(a) Aluminum reflector segments.



C-62539

(b) Control drum and poison plate.

Figure 3. Components of reflector assembly.

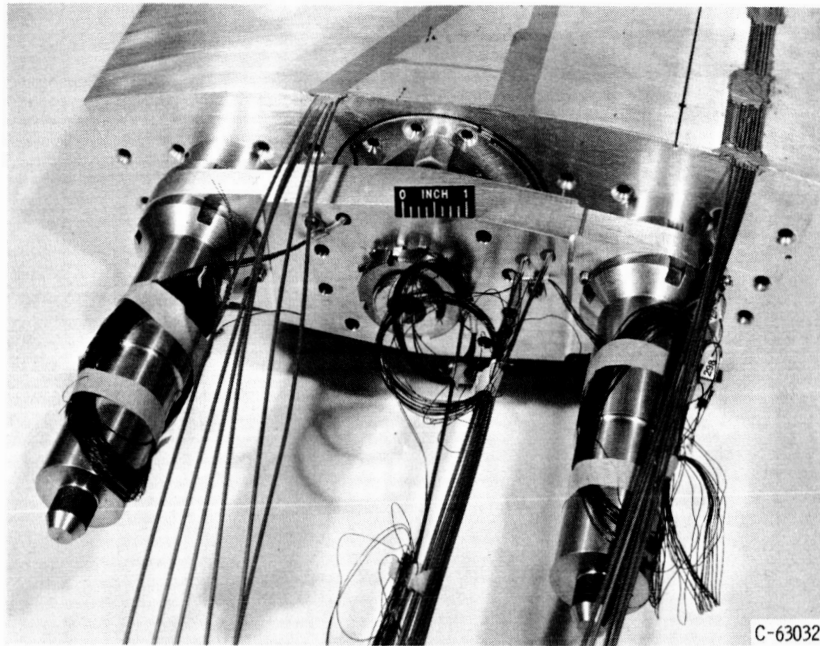


Figure 4. - Reflector-sector assembly (dome end) showing instrumentation leads.

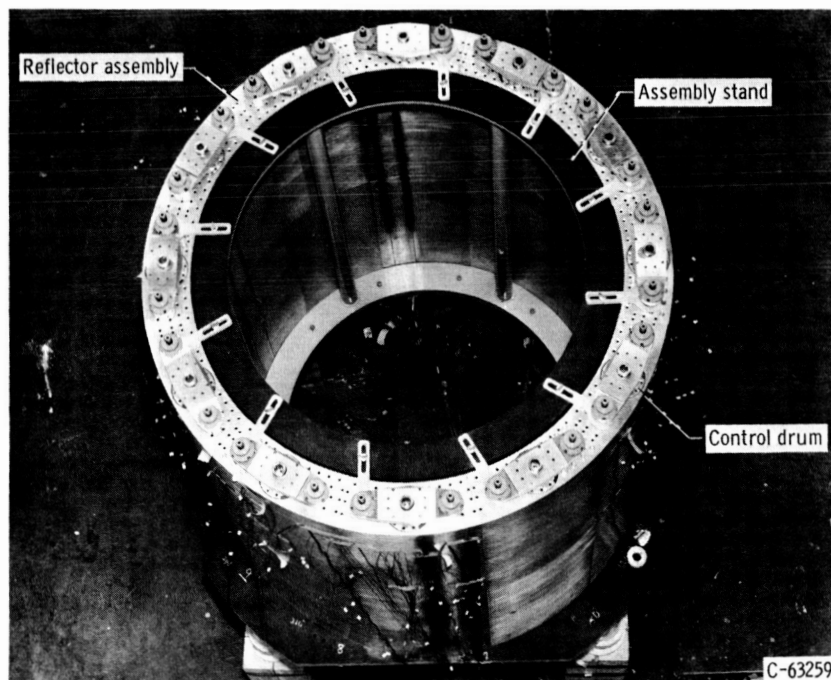
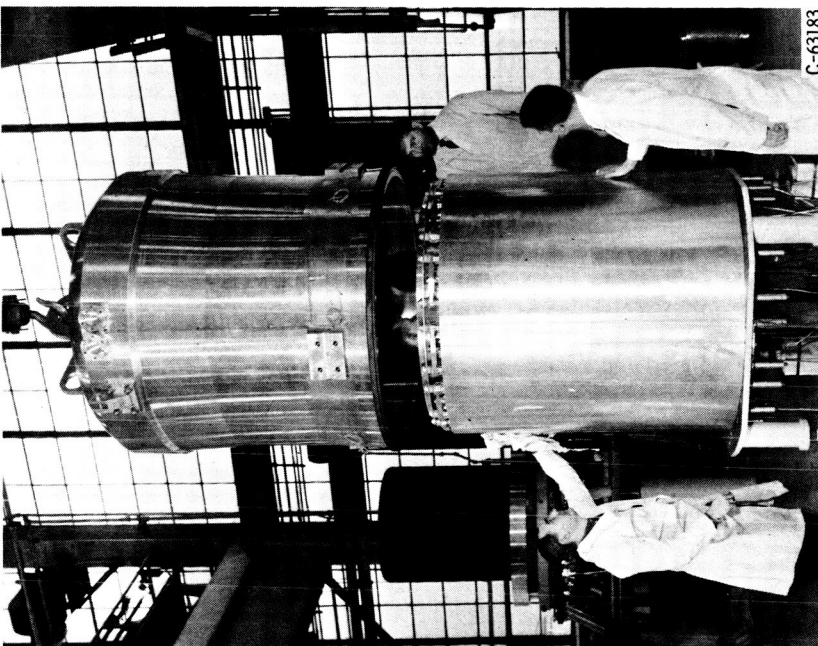
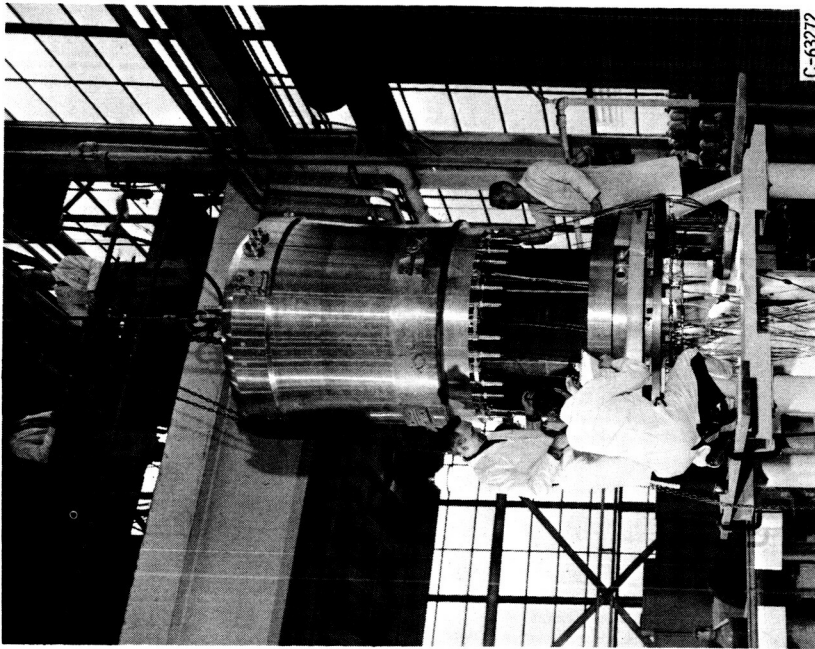


Figure 5. - Reflector-sector assembly in assembly stand.



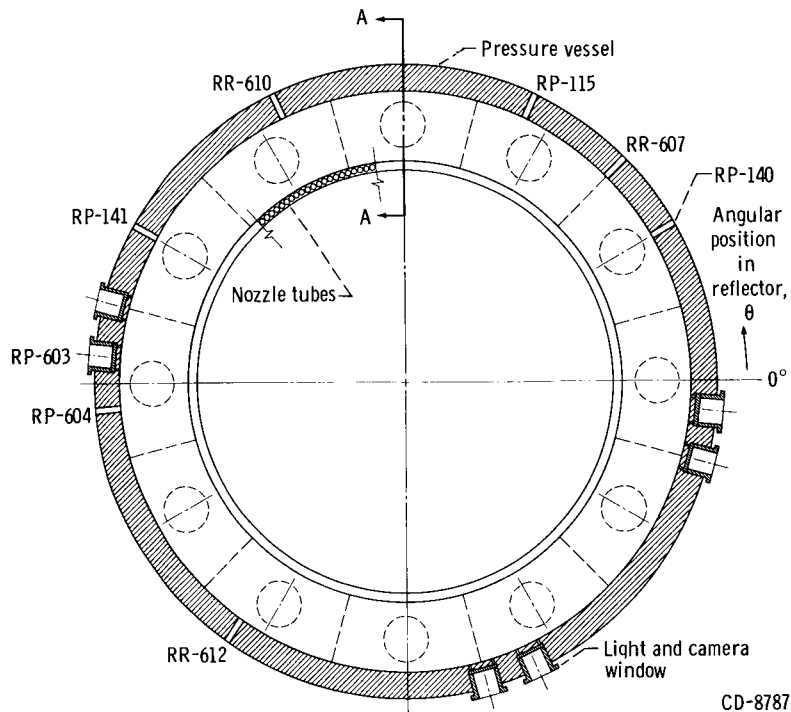
C-63183

Figure 6. - Lowering of pressure-vessel assembly over outer-reflector assembly.



C-63272

Figure 7. - Lowering of pressure vessel and outer-reflector assembly over core and inner-reflector assembly.



| Item designation | Axial distance from top of reflector, Z, in. | Angular position in reflector, θ , deg |
|--------------------|--|---|
| Fluid temperatures | | |
| RR-607 | 53 | 45 |
| RR-610 | 53 | 115 |
| RR-612 | 53 | 235 |
| Pressures | | |
| RP-140 | 53 | 40 |
| RP-141 | 53 | 150 |
| RP-603 | 57 | 175 |
| RP-604 | 57 | 185 |
| RP-115 | 53 | 65 |

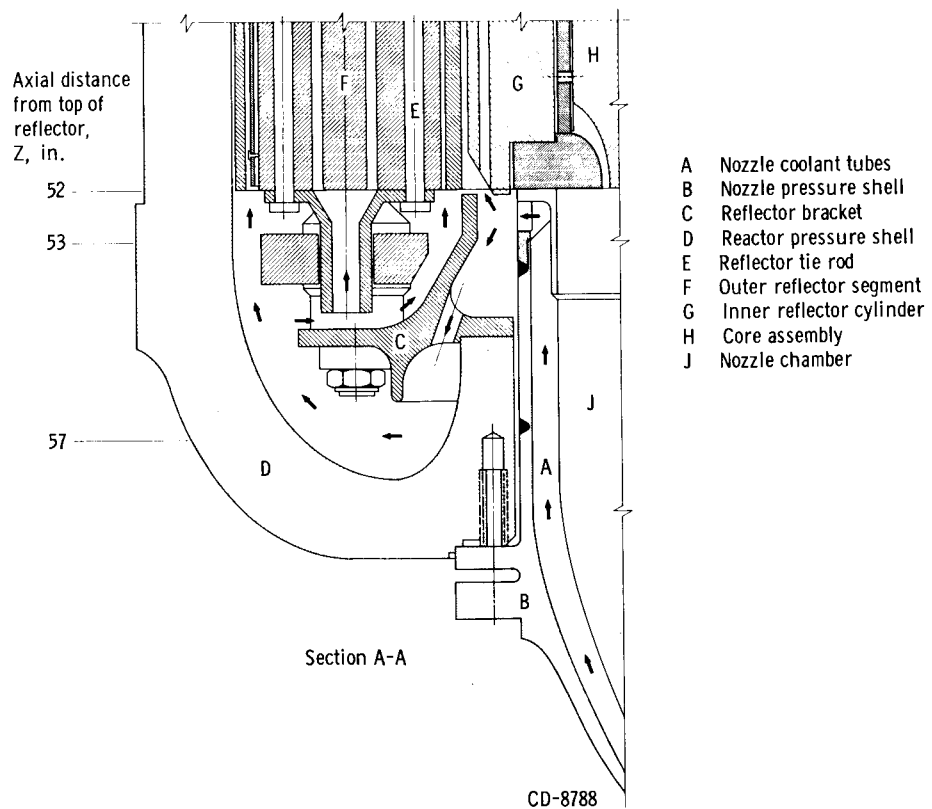
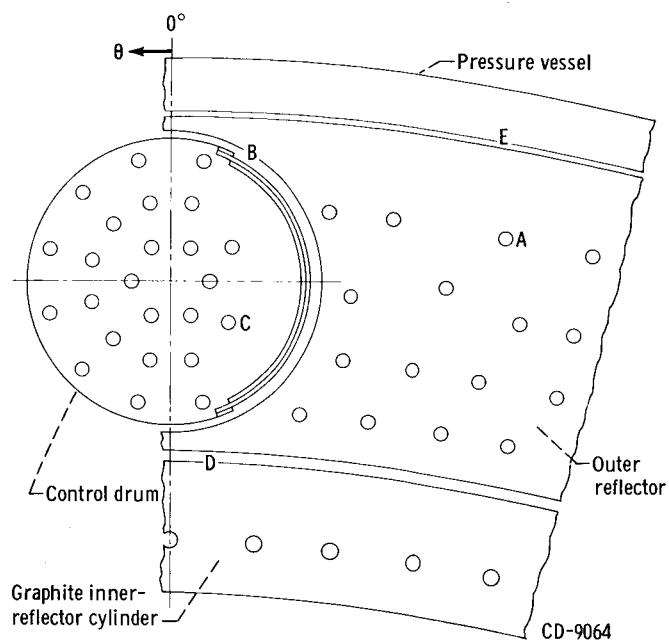
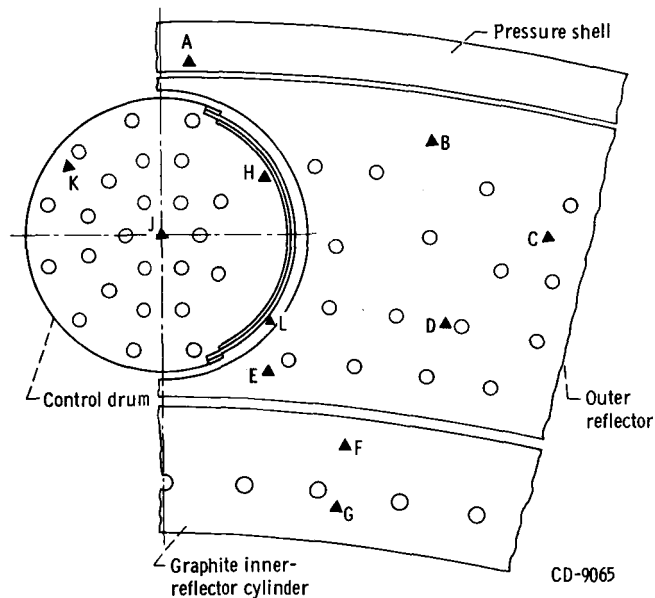


Figure 8. - Reflector-inlet plenum instrumentation (axial distance from top of reflector, 53 in. typical).



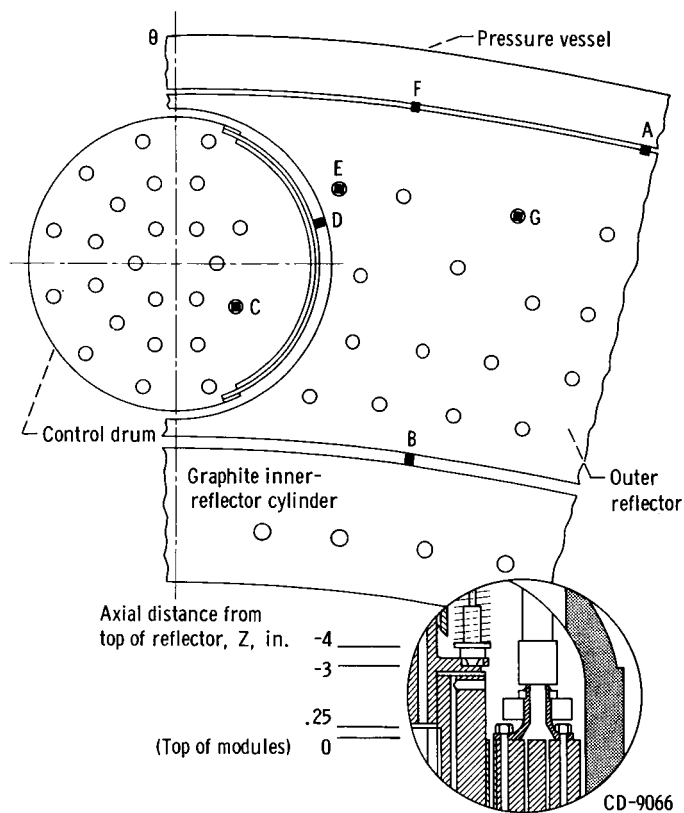
| Item designation | Angular position in reflector, θ , deg | Axial distance from top of reflector, Z , in. | Passage |
|------------------|---|---|---------|
| RP-58 | 348 | 1.25 | A |
| RP-66 | 168 | 13.25 | A |
| RP-68 | 168 | 36.25 | A |
| RP-70 | 357 | 1.25 | B |
| RP-103 | 357 | 1.25 | C |
| RP-117 | 330 | 1.25 | D |
| RP-124 | 350 | 1.00 | E |

Figure 9. - Reflector pressure instrumentation.



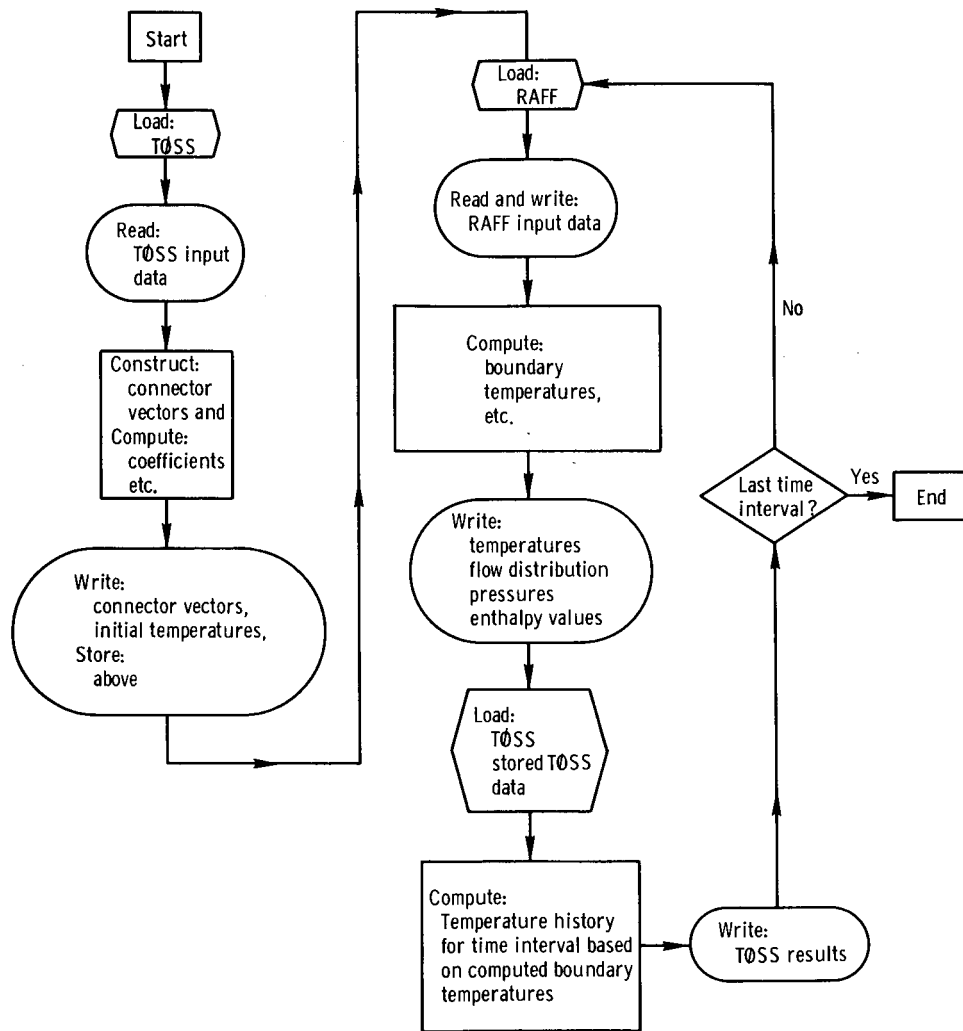
| Item designation | Axial distance from top of reflector, Z, in. | Angular position in reflector, θ , deg | Item designation | Axial distance from top of reflector, Z, in. | Angular position in reflector, θ , deg |
|------------------|--|---|------------------------|--|---|
| A | | | F | | |
| RT-388 | 1.5 | 350 | RT-95 | 1.25 | 350 |
| RT-389 | 28.5 | 350 | RT-96 | 28.25 | 350 |
| RT-390 | 51.5 | 350 | RT-97 | 49.38 | 350 |
| RT-380 | 28.5 | 170 | RT-77 | 1.25 | 170 |
| RT-383 | 28.5 | 230 | RT-78 | 28.25 | 170 |
| RT-386 | 28.5 | 290 | RT-79 | 49.38 | 170 |
| B | | | G | | |
| RT-104 | 1.25 | 350 ↓ | RT-94 | 49.62 | 350 |
| RT-105 | 16.25 | | | H | |
| RT-106 | 28.25 | | | | |
| RT-107 | 39.25 | | RT-269 | 2.25 | 356 |
| RT-108 | 45.25 | | RT-270 | 28.25 | 356 |
| RT-109 | 51.25 | | RT-271 | 50.25 | 356 |
| C | | | RT-386 | 28.25 | 290 |
| D | | | J | | |
| RT-116 | 1.25 | 346 ↓ | RT-263 | 2.5 | 0 |
| RT-117 | 16.25 | | RT-264 | 28.5 | 0 |
| RT-118 | 28.25 | | RT-265 | 50.0 | 0 |
| RT-119 | 39.25 | | RT-274 | 50.0 | 60 |
| RT-120 | 45.25 | | RT-283 | 50.0 | 120 |
| RT-121 | 51.25 | | RT-290 | 2.5 | 180 |
| E | | | RT-292 | 50.0 | 180 |
| RT-110 | 1.25 | 348 ↓ | RT-301 | 50.0 | 240 |
| RT-111 | 16.25 | | RT-310 | 50.0 | 300 |
| RT-112 | 28.25 | | K | | |
| RT-113 | 39.25 | | RT-266 | 2.25 | 4 |
| RT-234 | 45.25 | | RT-267 | 28.25 | 4 |
| RT-235 | 51.25 | | RT-268 | 50.25 | 4 |
| RT-206 | 1.25 | 229 | RT-293 | 2.25 | 184 |
| RT-208 | 28.25 | 229 | RT-295 | 50.25 | 184 |
| RT-211 | 51.25 | 229 | L (fluid temperatures) | | |
| F | | | RM-317 | 1.25 | 356 |
| RT-98 | 1.25 | 350 ↓ | RM-319 | 28.25 | 356 |
| RT-99 | 16.25 | | RM 321 | 45.25 | 356 |
| RT-100 | 28.25 | | | | |
| RT-101 | 39.25 | | | | |
| RT-126 | 45.25 | | 296 | | |
| RT-223 | 51.25 | | 236 | | |
| RT-194 | 1.25 | ↓ | | | |
| RT-196 | 28.25 | | | | |
| RT-199 | 51.25 | | | | |

Figure 10. - Reflector axial temperature sensor locations. Letters indicate position of thermocouples.



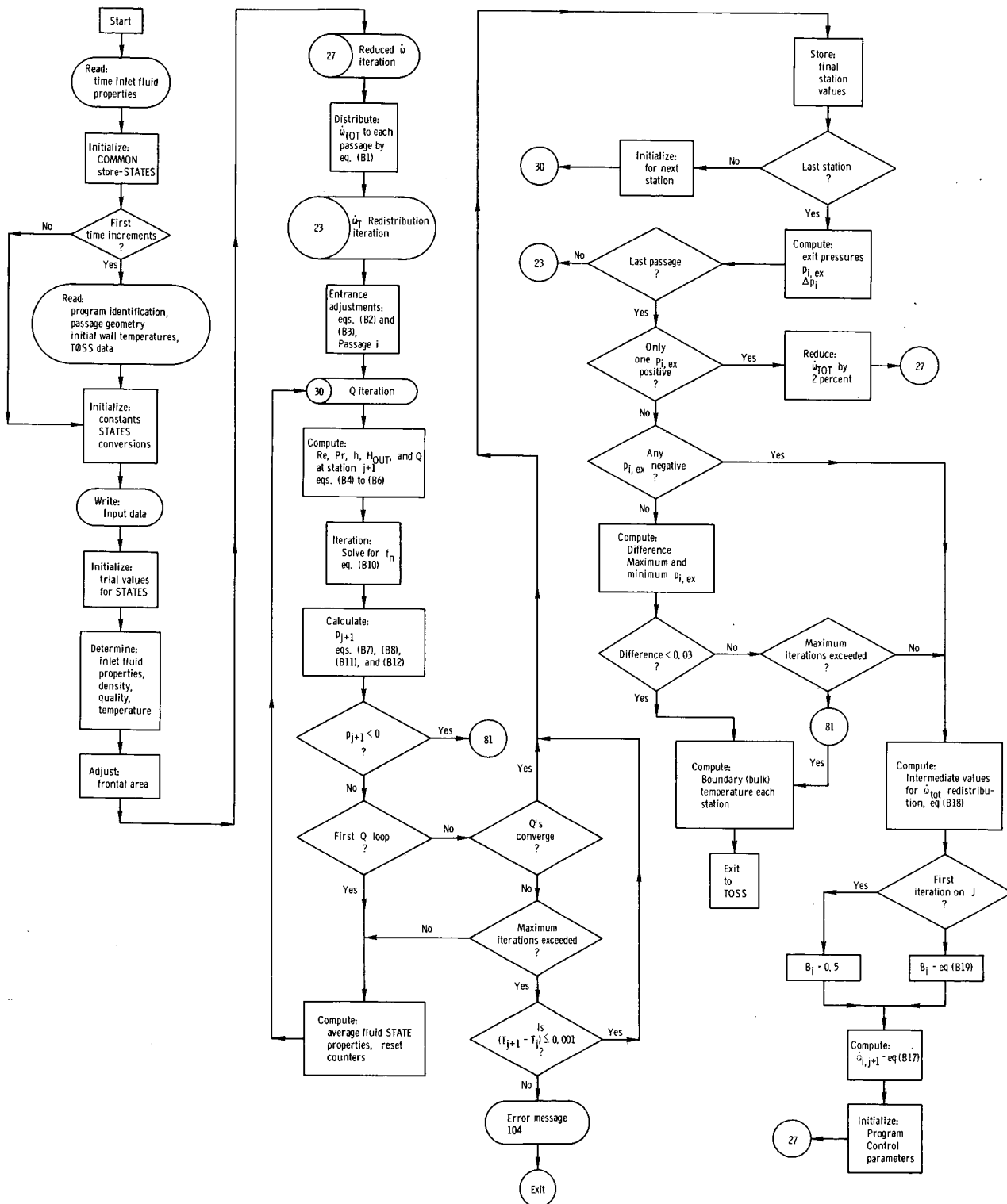
| Item designation | Axial distance from top of reflector, Z, in. | Angular position in reflector, θ , deg | Hole designation |
|--------------------|--|---|------------------|
| Fluid temperatures | | | |
| RR-619 | 45 | -3.00 | A |
| RT-260 | 349 | -.25 | B |
| RT-254 | 357 | -.25 | C |
| RT-257 | 356 | -.25 | D |
| RT-248 | 355 | -.25 | E |
| RR-622 | 115 | -3.00 | E |
| RT-622 | 115 | -3.00 | E |
| RR-624 | 235 | -3.00 | E |
| RT-245 | 354 | -.25 | F |
| RT-242 | 348 | -.25 | G |
| Pressures | | | |
| RP-145 | 30 | -3.0 | |
| RP-146 | 150 | -3.0 | |
| RP-147 | 270 | -3.0 | |
| RP-125 | 65 | -3.0 | |

Figure 11. - Reflector-outlet plenum instrumentation.



(a) Main flow chart.

Figure 12. - Multipassage fluid-flow code, RAFF.



(b) Detailed flow chart.
Figure 12. - Concluded.

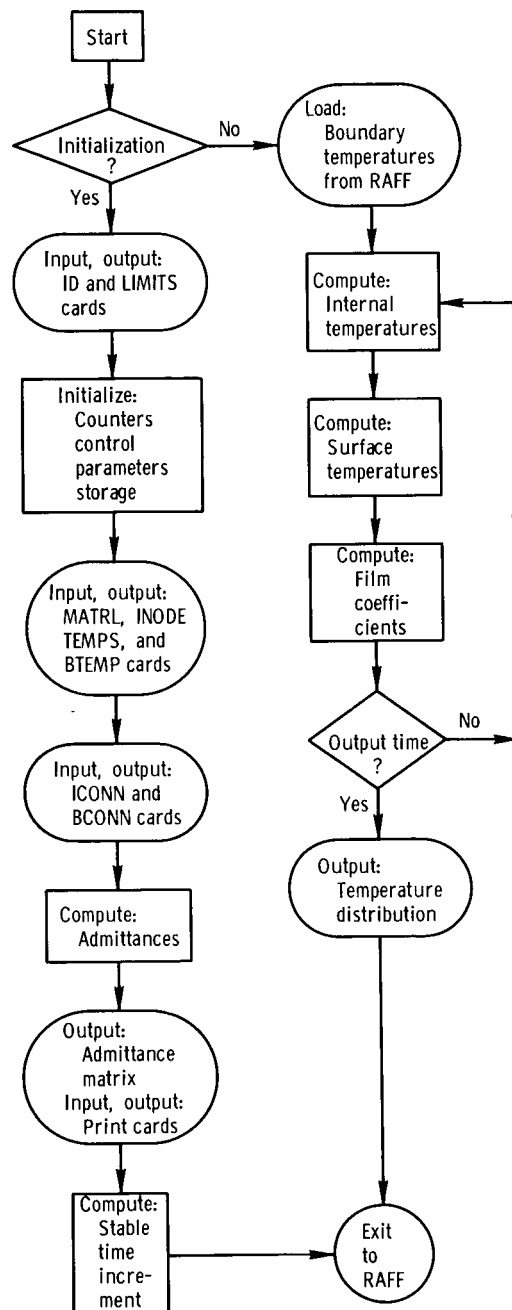
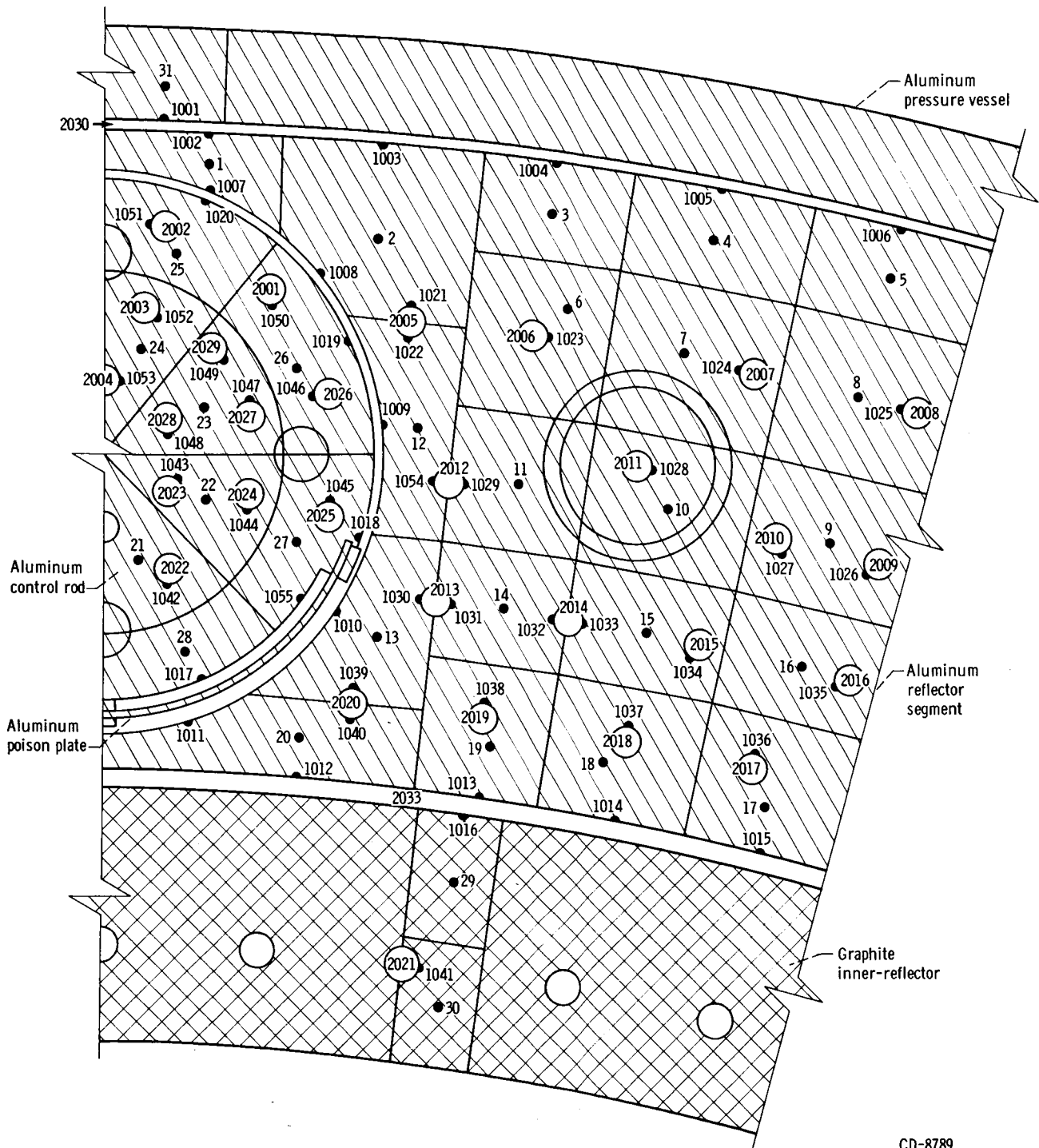
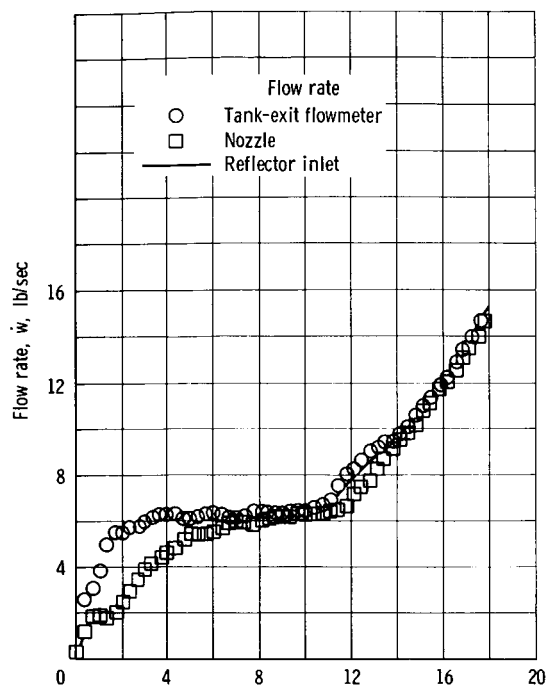


Figure 13. - TOSS flow chart.

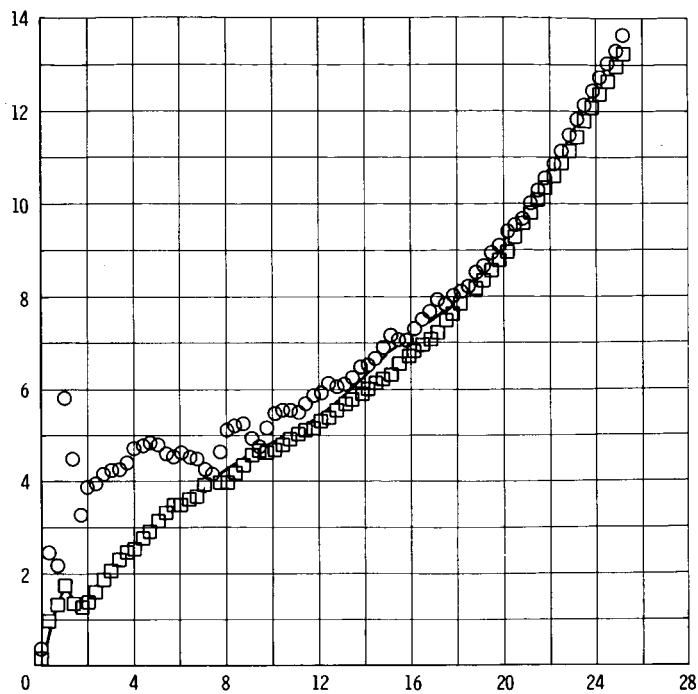


CD-8789

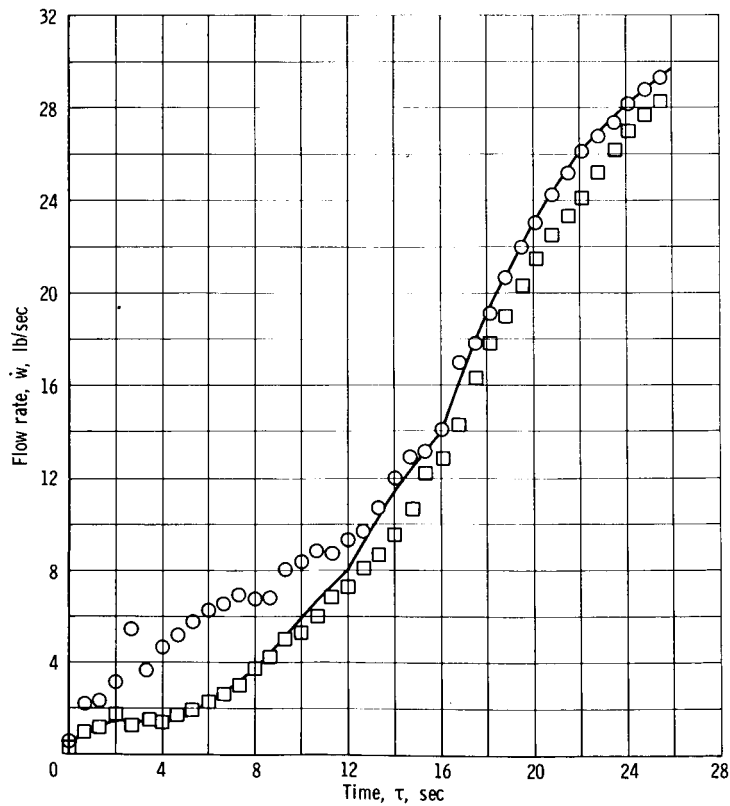
Figure 14. - Nodal description of 15° sector of reflector. Internal nodes, 1 to 31; surface nodes, 1001 to 1053; boundary nodes, 2001 to 2033.



(a) Run 11.

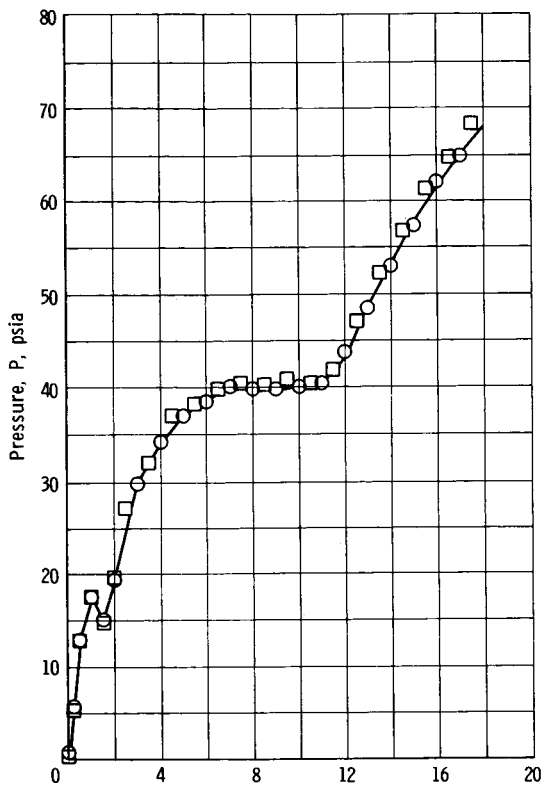


(b) Run 19.

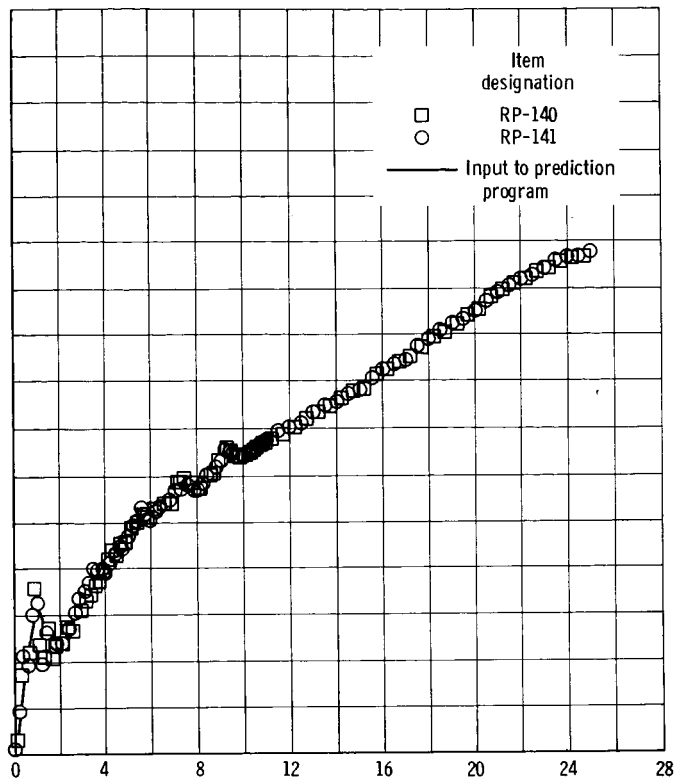


(c) Run 24.

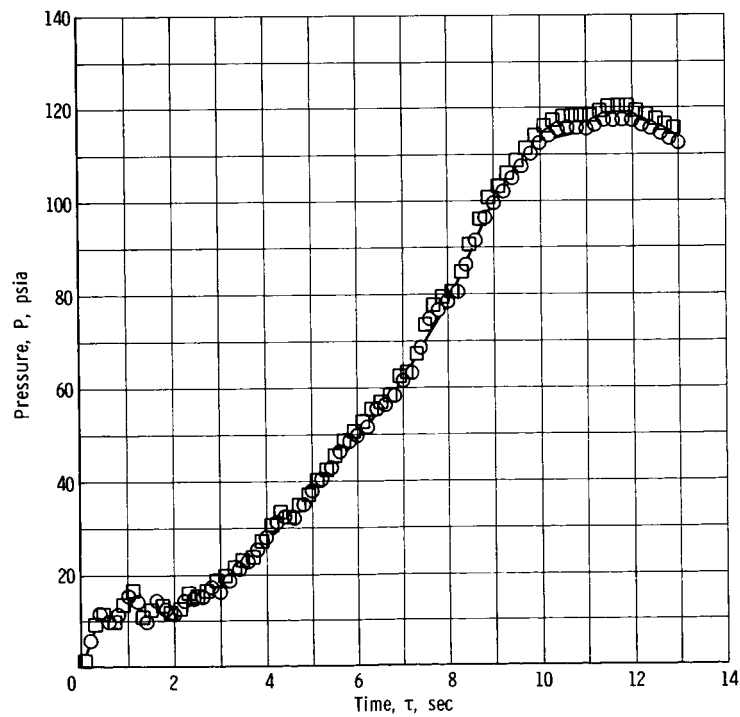
Figure 15. - Flow rate as function of time.



(a) Run 11.

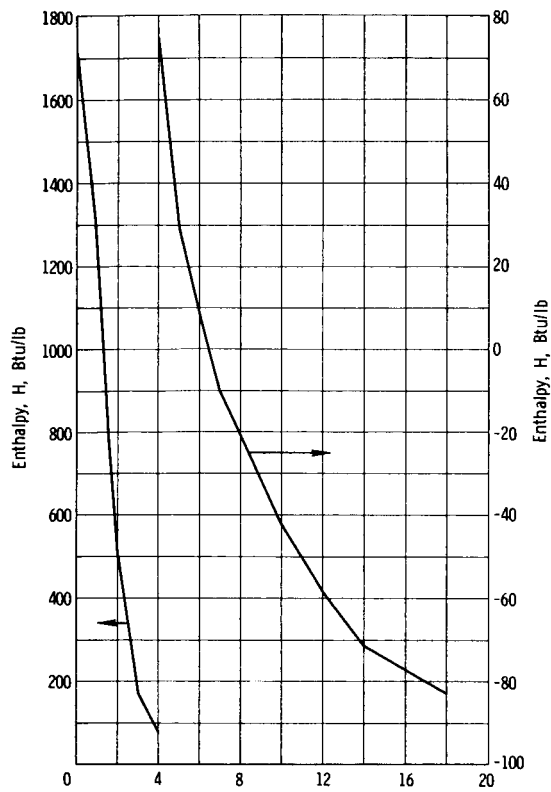


(b) Run 19.

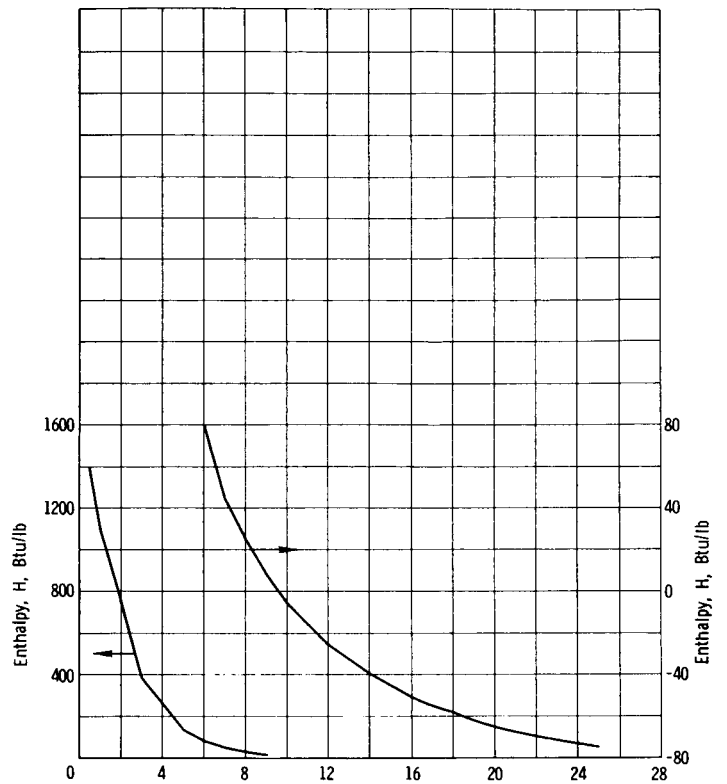


(c) Run 24.

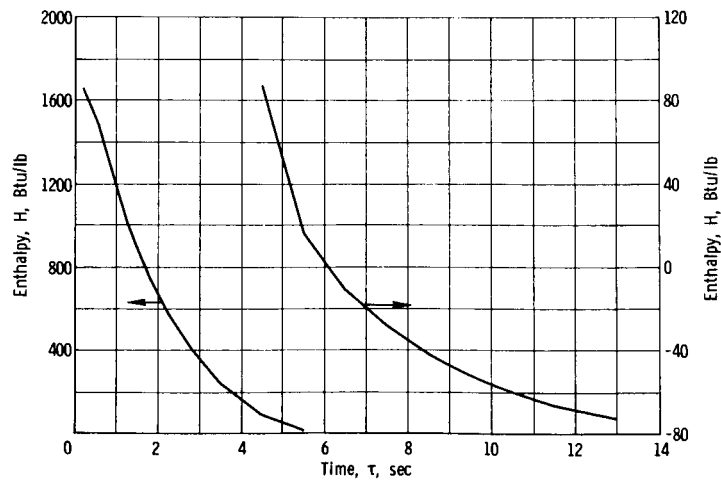
Figure 16. - Reflector inlet pressure as function of time.



(a) Run 11.

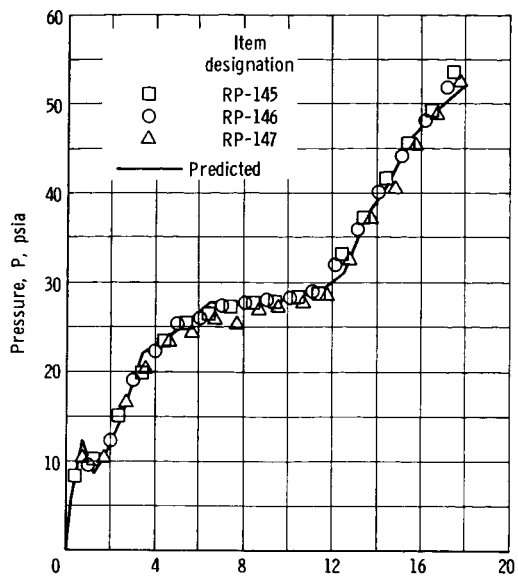


(b) Run 19.

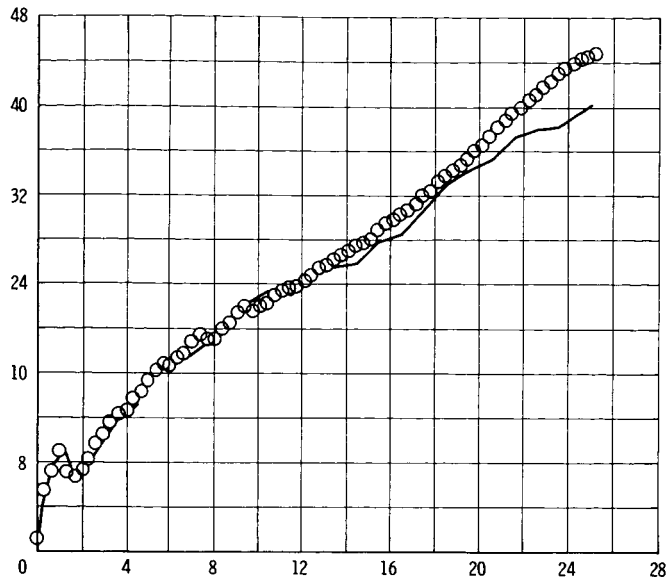


(c) Run 24.

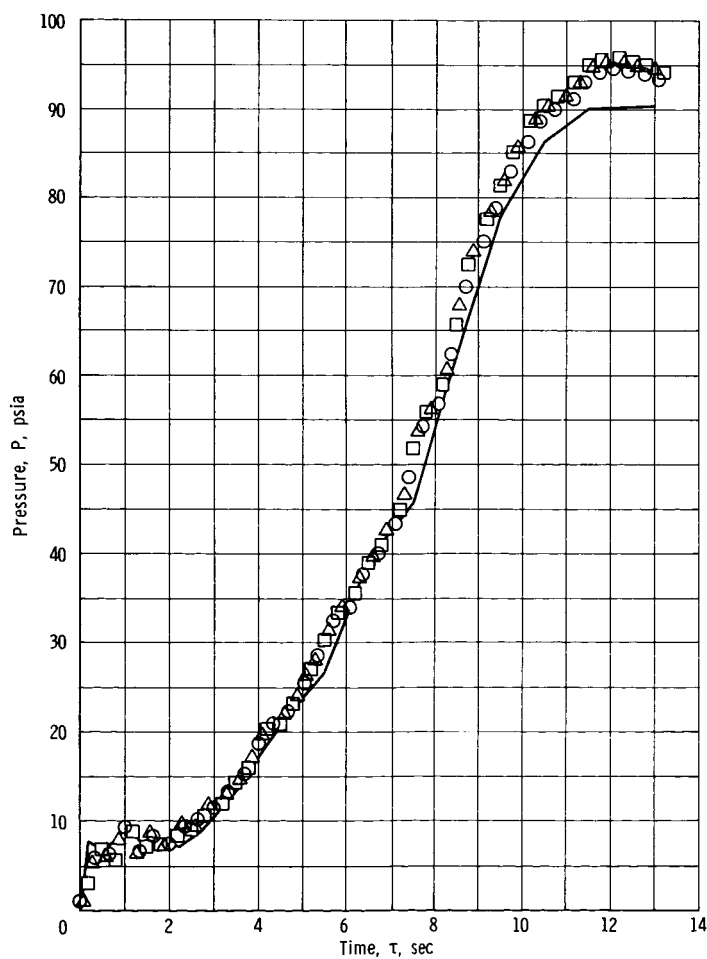
Figure 17. - Reflector-inlet enthalpy as function of time.



(a) Run 11.

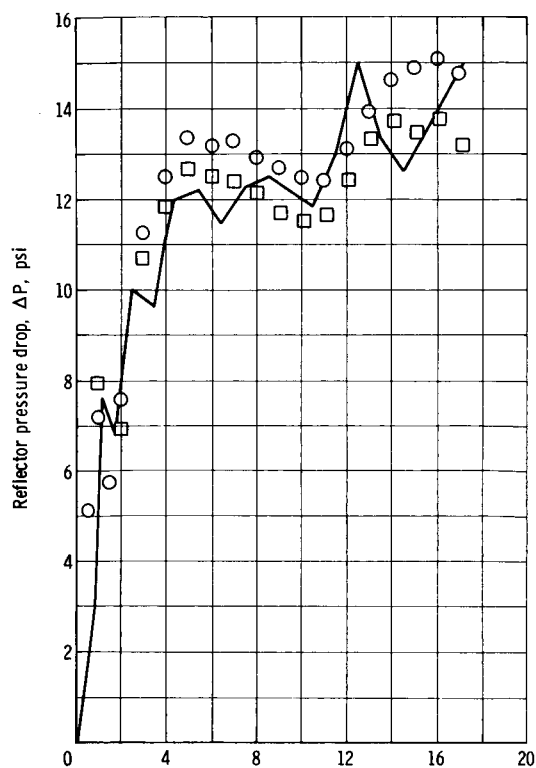


(b) Run 19.

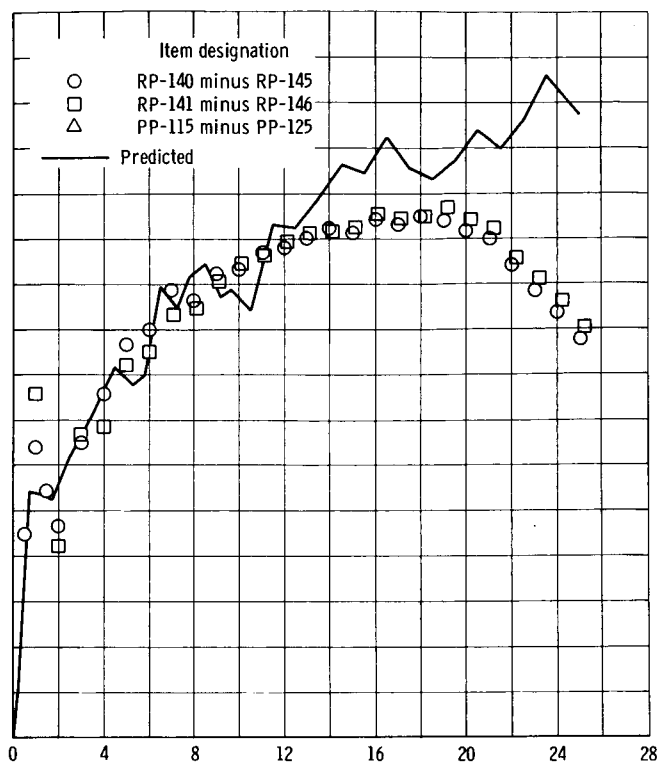


(c) Run 24.

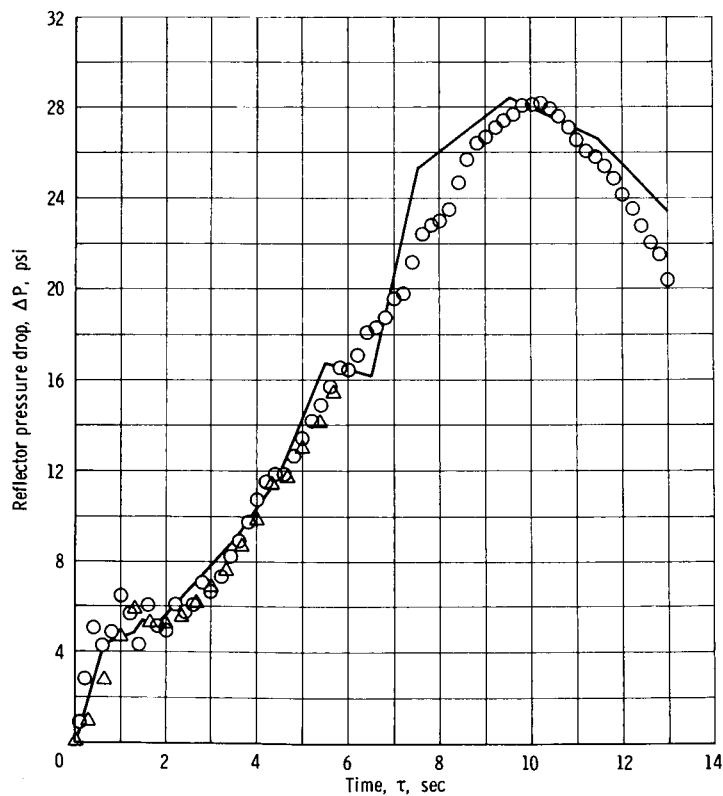
Figure 18. - Reflector-exit pressure as function of time.



(a) Run 11.

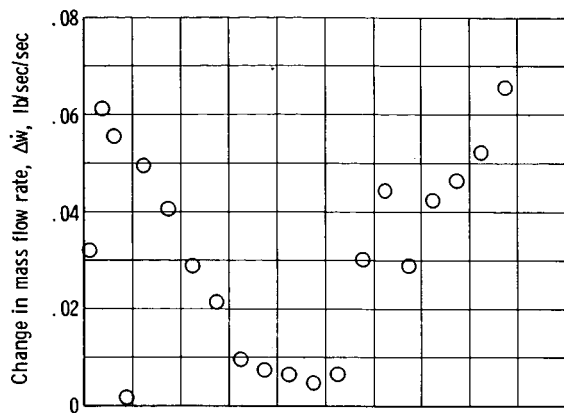


(b) Run 19.

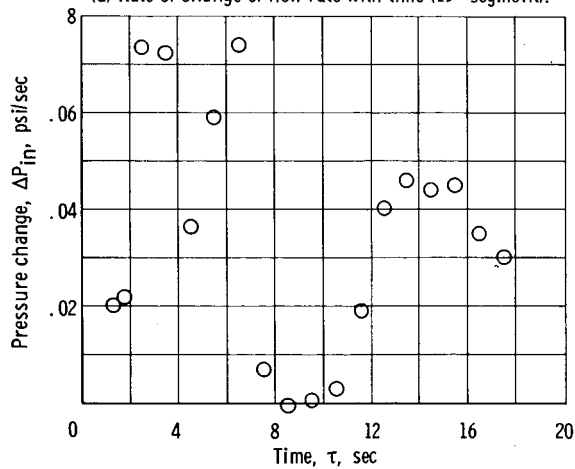


(c) Run 24.

Figure 19. - Reflector pressure drop as function of time.

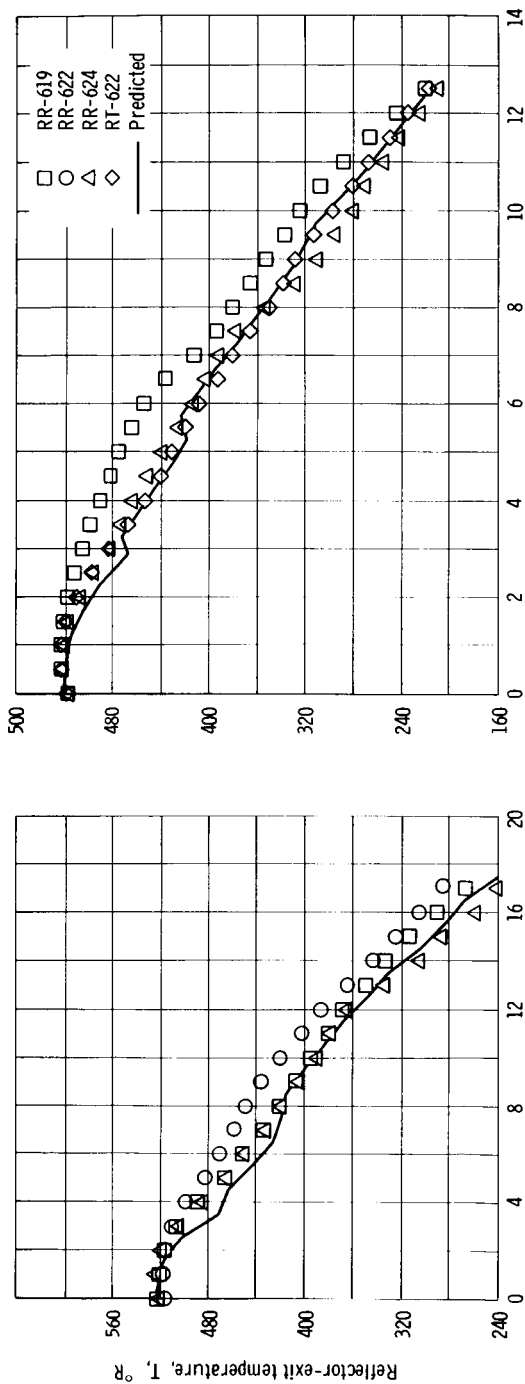


(a) Rate of change of flow rate with time (15° segment).



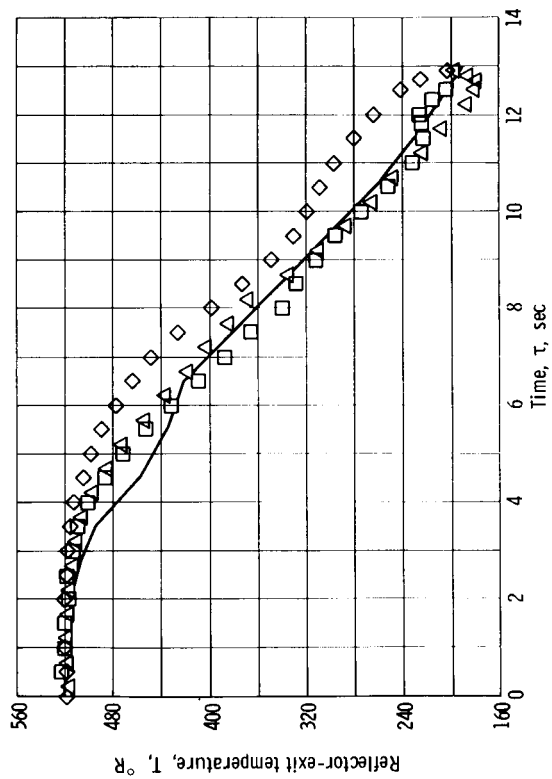
(b) Rate of change of inlet pressure with time.

Figure 20. - Rate of change of flow rate and inlet pressure as function of time. Run 11.



(a) Run 11.

(b) Run 19.



(c) Run 24.

Figure 21. - Reflector-exit fluid temperature as function of time.

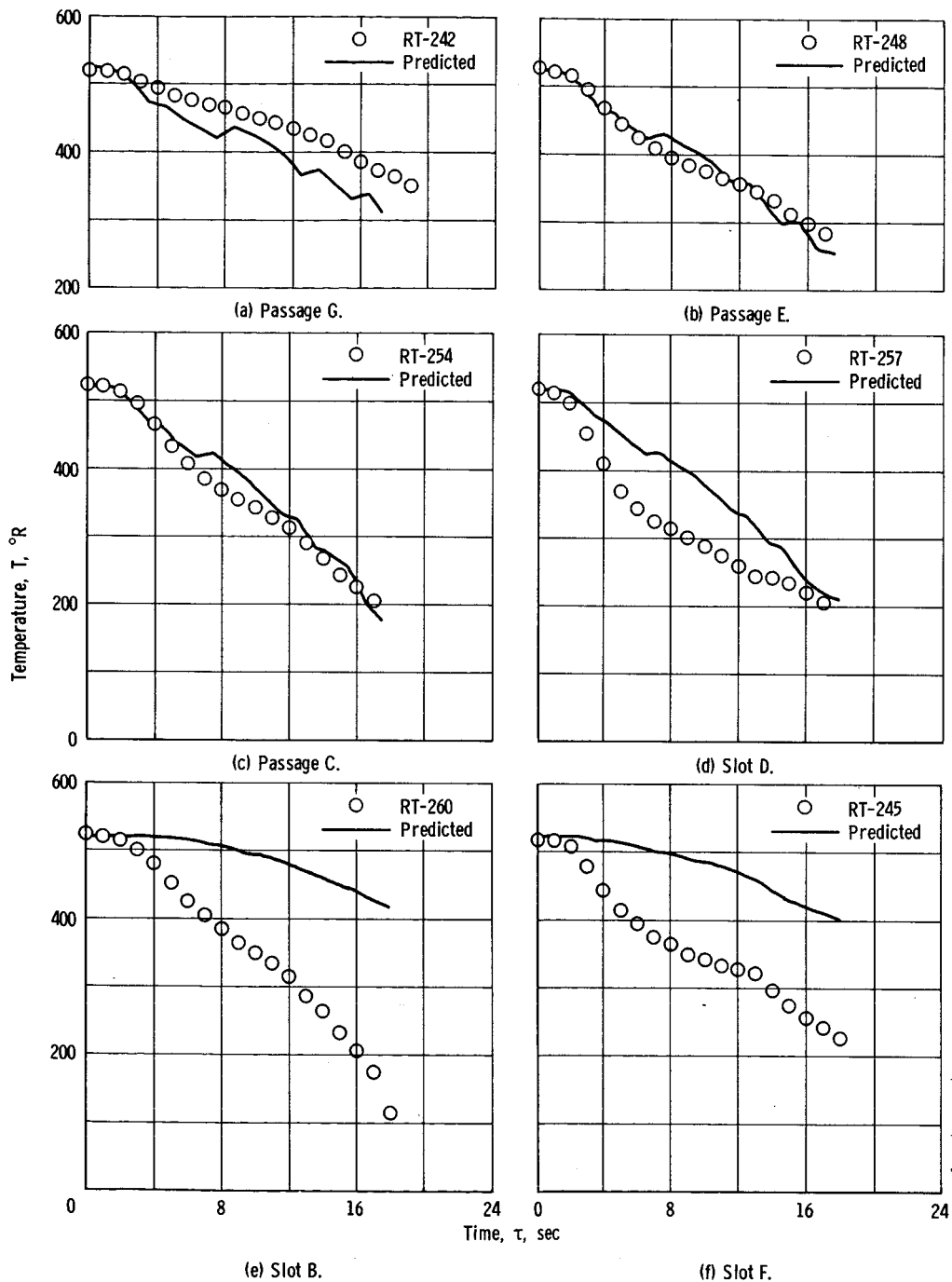


Figure 22. - Reflector-passage exit temperature history for several passages. Run 11. (See fig. 11.)

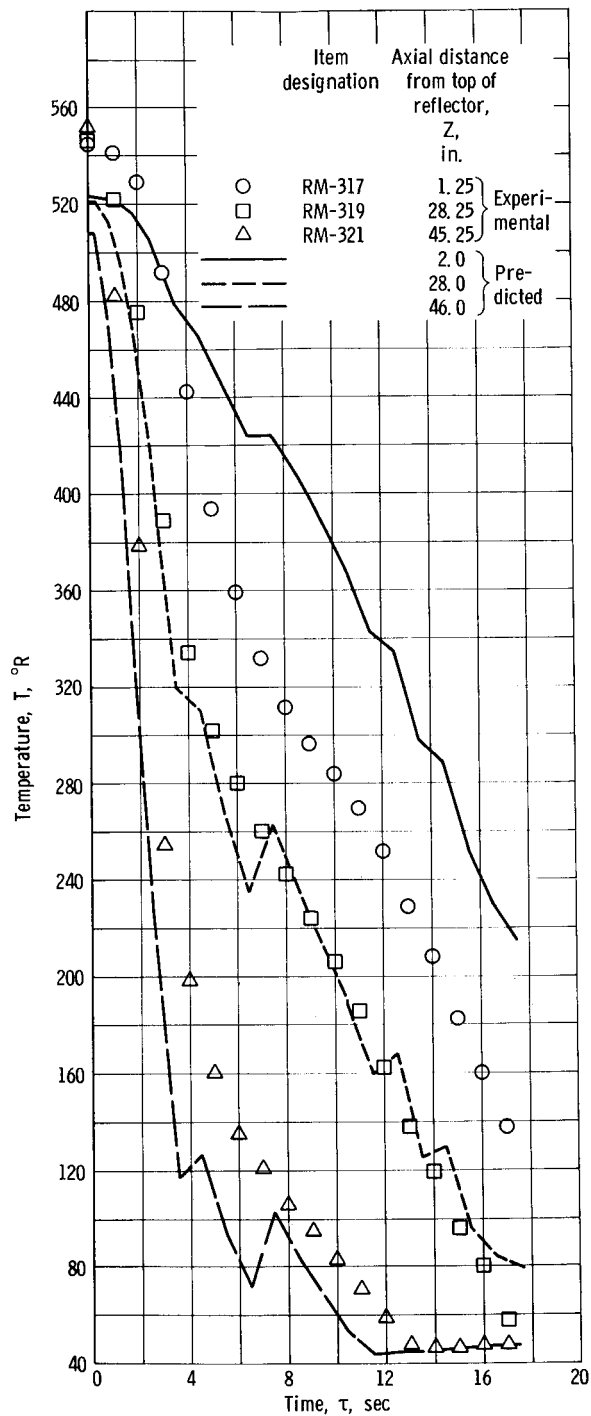
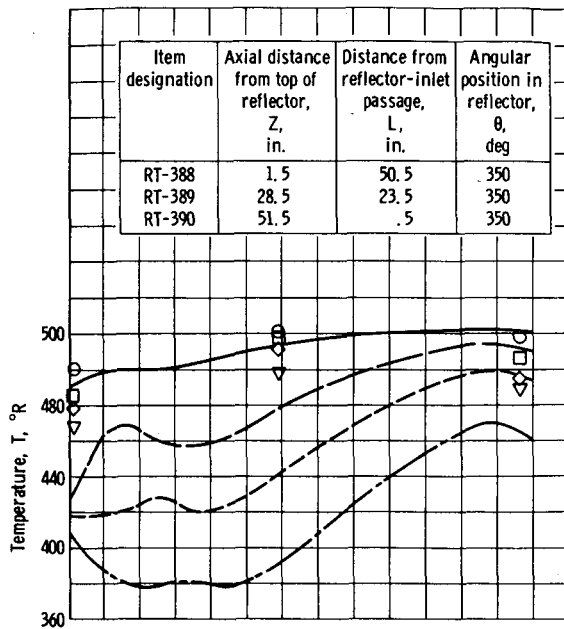
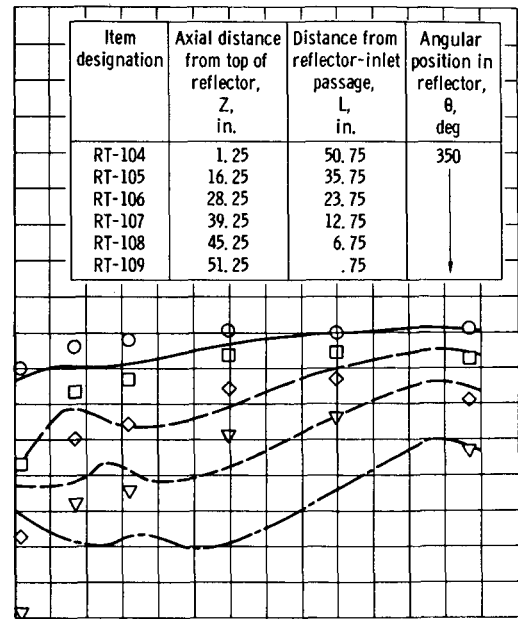


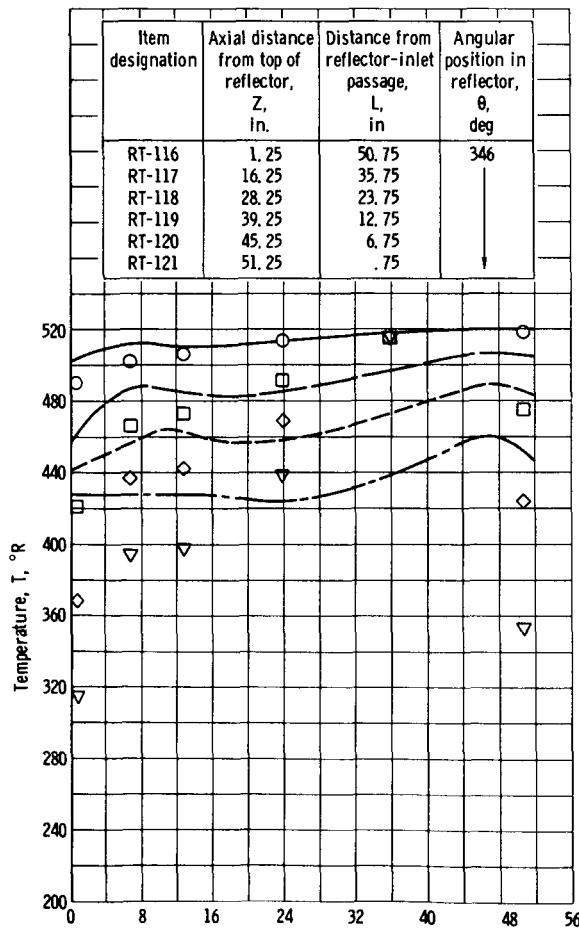
Figure 23. - Fluid temperature as function of time within control drum slot (see fig. 10). Run 11.



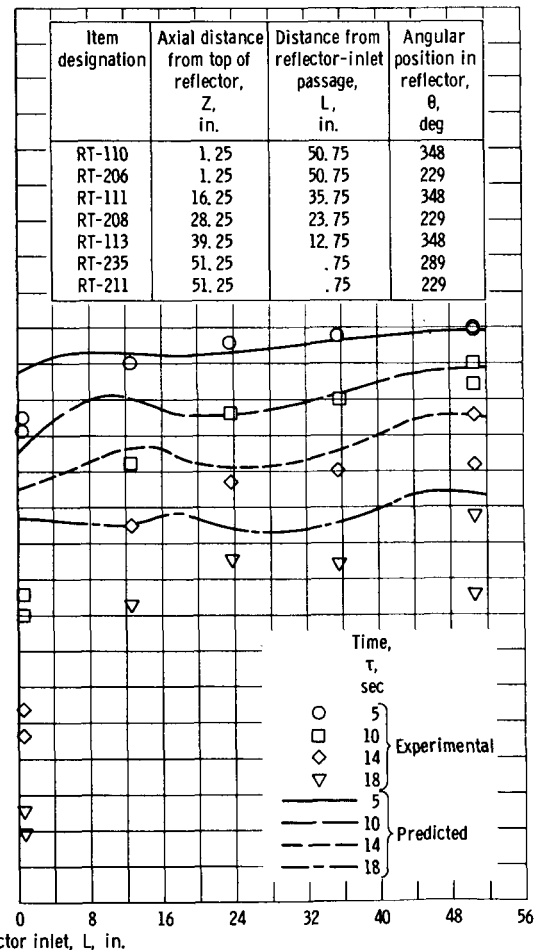
(a) Location A, pressure vessel.



(b) Location B, outer-reflector segment.

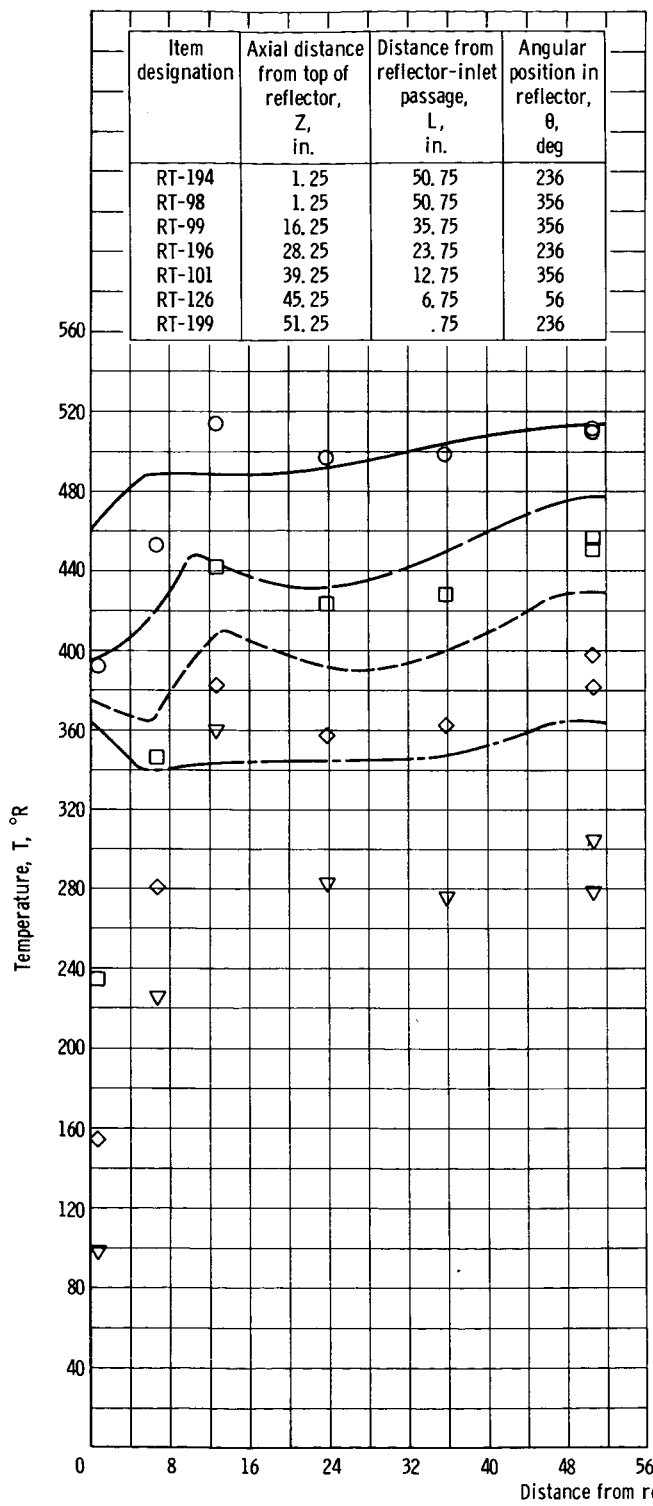


(c) Location C, outer-reflector segment.

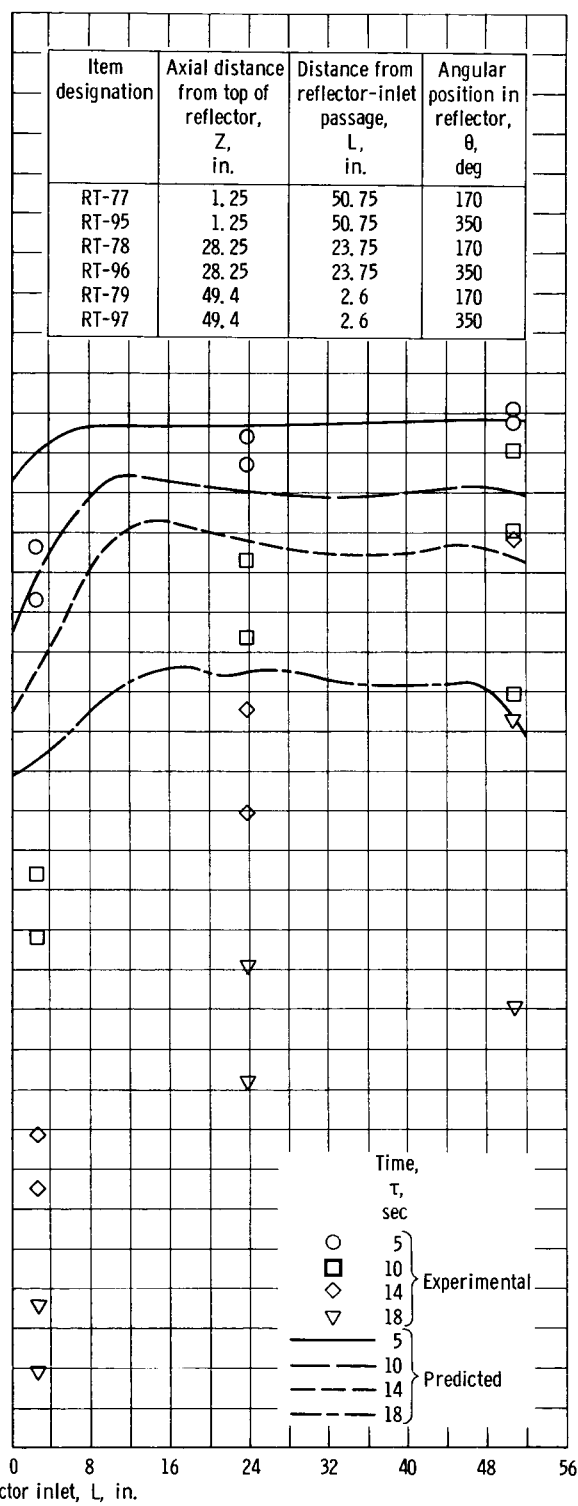


(d) Location D, outer-reflector segment.

Figure 25. - Axial material temperature distribution (see fig. 10). Run 11.

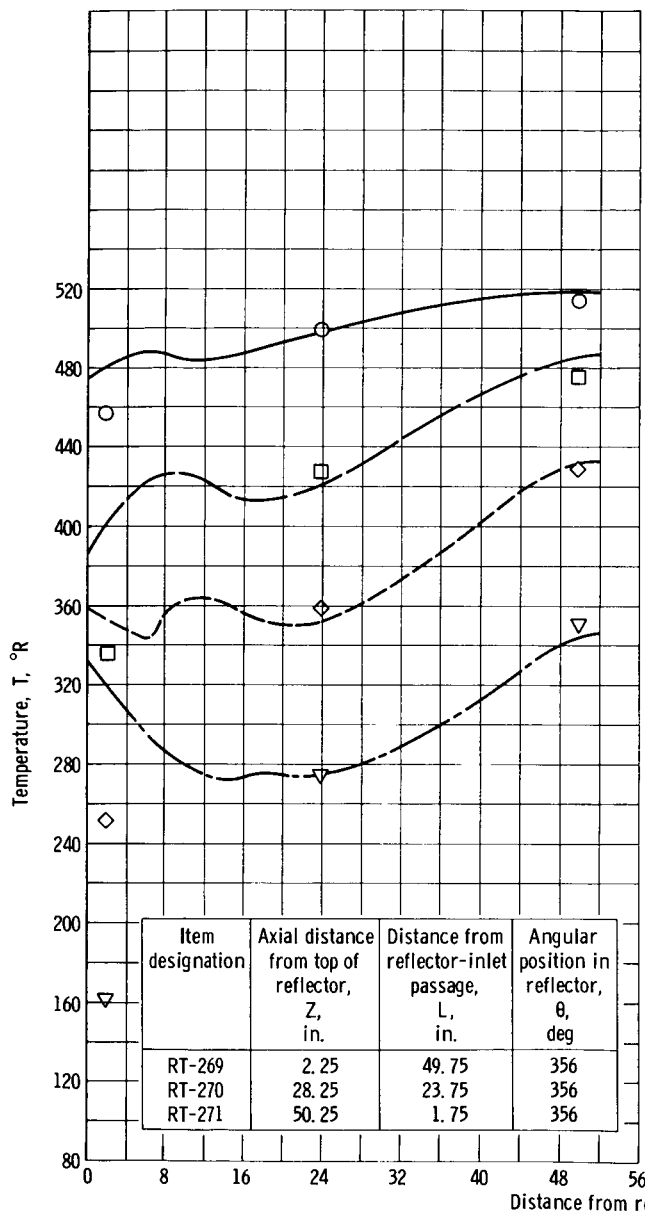


(e) Location E, outer-reflector segment.

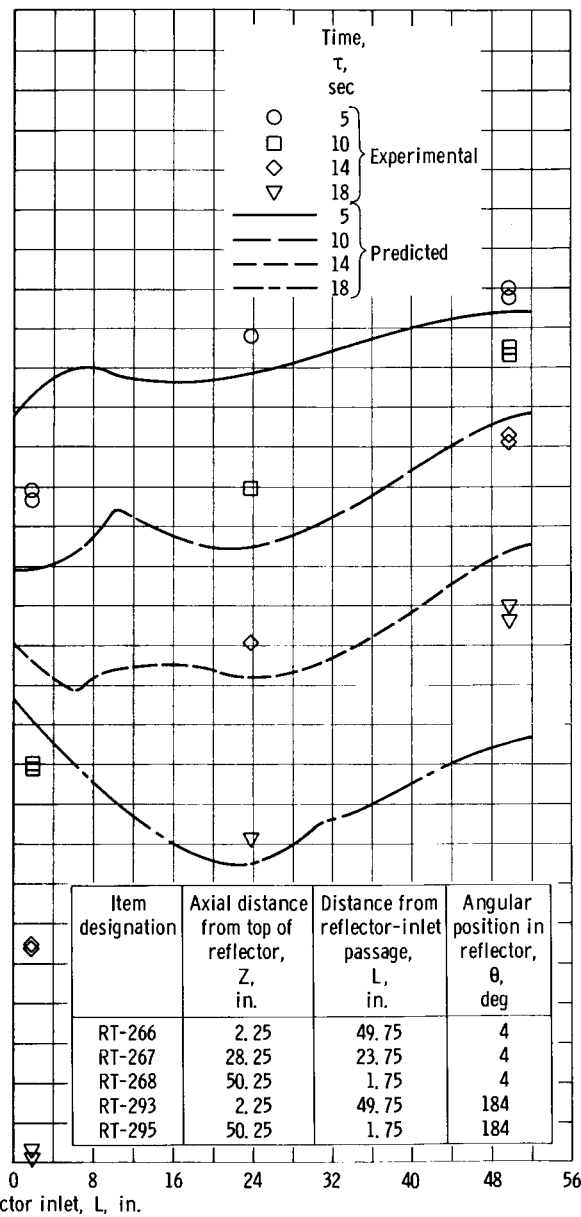


(f) Location F, graphite reflector cylinder.

Figure 25. - Continued.



(g) Location H, control drum.



(h) Location K, control drum.

Figure 25. - Continued.

~~CONFIDENTIAL~~

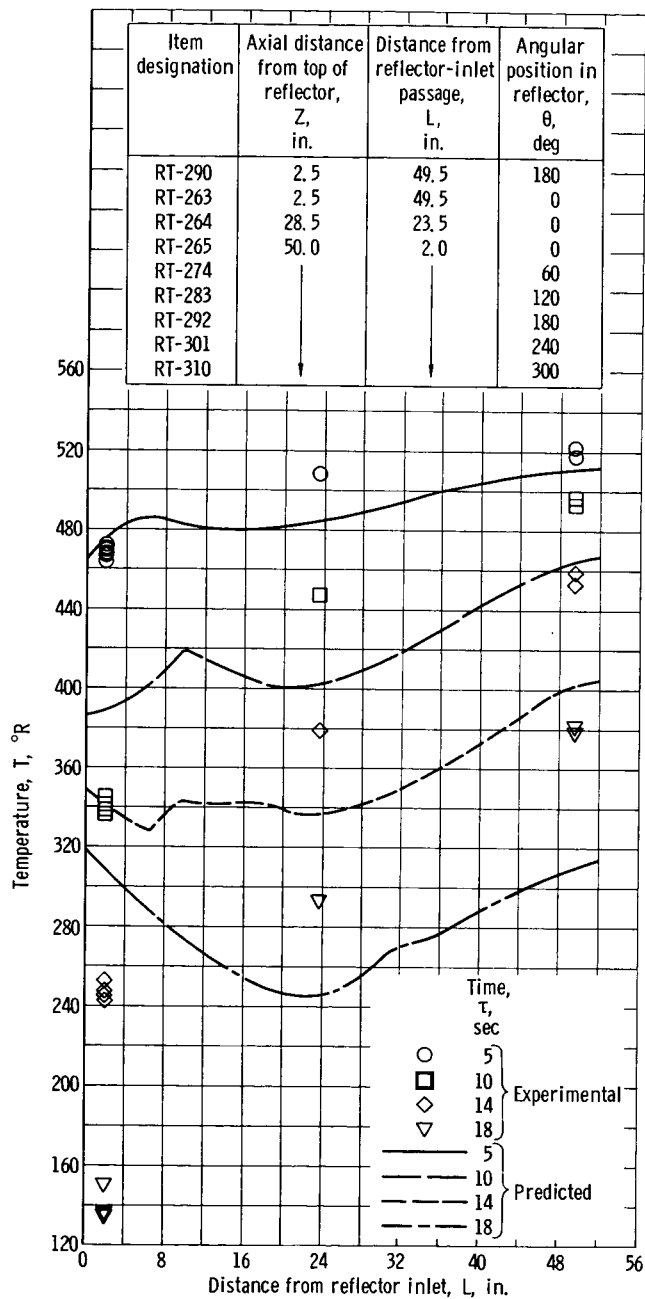


Figure 25. - Concluded.

~~CONFIDENTIAL~~

[REDACTED]

"The aeronautical and space activities of the United States shall be conducted so as to contribute . . . to the expansion of human knowledge of phenomena in the atmosphere and space. The Administration shall provide for the widest practicable and appropriate dissemination of information concerning its activities and the results thereof."

—NATIONAL AERONAUTICS AND SPACE ACT OF 1958

NASA SCIENTIFIC AND TECHNICAL PUBLICATIONS

TECHNICAL REPORTS: Scientific and technical information considered important, complete, and a lasting contribution to existing knowledge.

TECHNICAL NOTES: Information less broad in scope but nevertheless of importance as a contribution to existing knowledge.

TECHNICAL MEMORANDUMS: Information receiving limited distribution because of preliminary data, security classification, or other reasons.

CONTRACTOR REPORTS: Scientific and technical information generated under a NASA contract or grant and considered an important contribution to existing knowledge.

TECHNICAL TRANSLATIONS: Information published in a foreign language considered to merit NASA distribution in English.

SPECIAL PUBLICATIONS: Information derived from or of value to NASA activities. Publications include conference proceedings, monographs, data compilations, handbooks, sourcebooks, and special bibliographies.

TECHNOLOGY UTILIZATION PUBLICATIONS: Information on technology used by NASA that may be of particular interest in commercial and other non-aerospace applications. Publications include Tech Briefs, Technology Utilization Reports and Notes, and Technology Surveys.

Details on the availability of these publications may be obtained from:

SCIENTIFIC AND TECHNICAL INFORMATION DIVISION
NATIONAL AERONAUTICS AND SPACE ADMINISTRATION

Washington, D.C. 20546

[REDACTED]